POLITECNICO DI TORINO
Repository ISTITUZIONALE

An Intensity Measure-Based Methodology for Ground Motion Orientation in Seismic Structural Assessment

Original
An Intensity Measure-Based Methodology for Ground Motion Orientation in Seismic Structural Assessment / Londono-Lopez, S., Cucuzza, R., Mollaioli, F., Marano, G.C., Domaneschi, M.. - In: EARTHQUAKE ENGINEERING & STRUCTURAL DYNAMICS. - ISSN 0098-8847. - (2026), pp. 1-21. [10.1002/eqe.70286]

Availability:
This version is available at: 11583/3016274 since: 2026-10-03T21:38:54Z

Publisher:
John Wiley and Sons

Published
DOI:10.1002/eqe.70286

Terms of use:

This article is made available under terms and conditions as specified in the corresponding bibliographic description in the repository

Publisher copyright

(Article begins on next page)

24 October 2026

Check for updates

Earthquake Engineering & Structural Dynamics

WILEY

RESEARCH ARTICLE OPEN ACCESS

An Intensity Measure-Based Methodology for Ground Motion Orientation in Seismic Structural Assessment

Santiago Londono-Lopez[1] | Raffaele Cucuzza[2] | Fabrizio Mollaioli[3] | Giuseppe Carlo Marano[2] | Marco Domaneschi[1,4]

[1]Department of Structural, Building and Geotechnical Engineering (DISEG), Politecnico di Torino, Turin, Italy | [2]School of Civil Engineering, Henan University of Technology, Zhengzhou, Henan Province, China | [3]Department of Structural and Geotechnical Engineering, Sapienza Università di Roma, Rome, Italy | [4]School of Civil Engineering, Southeast University, Nanjing, China

Correspondence: Raffaele Cucuzza (raffaele.cucuzza@polito.it) | Marco Domaneschi (marco.domaneschi@polito.it)

Received: 22 February 2026 | **Revised:** 29 June 2026 | **Accepted:** 17 August 2026

Keywords: engineering demand parameters | nonlinear time-history analysis | peak-polar rotation-intensity ordinates | seismic directionality

ABSTRACT

In current dynamic time history assessment protocols, ground motion recordings are mostly oriented along fixed sensor directions. Consequently, the orientation of the principal resultant of rupture energy, which may control the maximum structural demand, remains undefined, precluding consistent correlation with physically detrimental directivity effects. This study introduces the Peak-Polar Rotation–Intensity Ordinates methodology as a deterministic, intensity-measure-based orientation criterion for bidirectional ground motions in nonlinear time-history analysis. The method identifies record-specific principal directions by maximizing scalar intensity measures, namely Peak Ground Acceleration, Arias Intensity, Cumulative Absolute Velocity and Specific Energy Density. This approach is evaluated through statistical analysis of over 3400 pairs of recording of Far-Field, Near-Field, and Pulse-Like seismological regimes, utilizing an eight-storey reinforced concrete frame as a representative application for nonlinear time-history analysis. The investigation reveals a regime-dependency: while Far-Field motions exhibit tendencies toward isotropy, Pulse-Like events display stronger directional polarization tendency. For the Pulse-Like subset, Peak-Polar Rotation–Intensity Ordinates based on cumulative intensity measures, particularly Cumulative Absolute Velocity and Specific Energy Density, generally produced the largest storey-drift and roof-displacement demands among the considered orientation protocols. In representative cases, the maximum storey-drift demand reached approximately twice that obtained from the fault-oriented configuration. By replacing arbitrary geometric conventions with reproducible intensity-measure-based orientations, the proposed methodology provides a complementary tool for identifying potentially more demanding ground-motion alignments in bidirectional NLTHA.

1 | Introduction

Despite the complex dynamics governing earthquake generation and wave propagation, the accurate modeling of ground motion remains a cross-cutting issue in the vulnerability assessment of the built environment [1, 2]. Particularly, Nonlinear time-history analysis (NLTHA) of three-dimensional structural systems requires the simultaneous application of two horizontal ground-motion components. Although this operation is standard in specialized engineering practices, the orientation of the bidirectional input relative to the structural axes remains a non-trivial modeling choice [3, 4]. The two recorded horizontal components are usually allocated along sensor axes, whereas alternative reference systems may be defined by fault-normal (FN)/fault-parallel(FP) directions, structural principal axes, or fixed-angle rotations of the as-recorded ground-motion pair. Consequently, the same bidirectional accelerogram may induce different linear/nonlinear force-deformation paths, different combinations

This is an open access article under the terms of the Creative Commons Attribution License, which permits use, distribution and reproduction in any medium, provided the original work is properly cited.
© 2026 The Author(s). *Earthquake Engineering & Structural Dynamics* published by John Wiley & Sons Ltd.

of biaxial member demands, and different peak engineering demand parameters depending only on the adopted incidence angle, particularly when post-elastic bidirectional interaction and local member deformation demands are activated [5, 6].

This issue is particularly relevant for NLTHA because nonlinear structural response is path-dependent. In linear response-spectrum analysis, directional effects can be partially addressed through modal combination rules or component combination factors [7]. In nonlinear dynamic analysis, however, the full acceleration histories are integrated in time, and the direction of the input motion may affect the evolution of inelastic demand, including yielding sequence, stiffness degradation, torsional coupling, residual displacement, local strain demand, and collapse-relevant displacement demand [8]. Therefore, the orientation of the horizontal components cannot be regarded as a simple post-processing convention; it is part of the seismic input definition.

Current engineering practice commonly adopts one of three approaches. The first is to apply the two horizontal components along their as-recorded sensor axes. The second is to rotate the record into a fault-based reference system, typically FN and FP, when fault geometry is available. The third is to perform a small number of fixed geometric rotations, such as 10° increments, relative to a selected reference frame. Each approach has advantages, but none necessarily identifies the orientation that produces high nonlinear structural demand. The as-recorded orientation depends on accelerometer installation rather than source, path, site, or structural characteristics. The FN/FP orientation is physically meaningful for near-fault directivity studies, but it is not, by definition, the orientation of maximum shaking or maximum structural response. Fixed-angle rotations are simple to implement, but they represent sparse samples of the directional response space and may miss the critical incidence angle.

Recent studies have demonstrated that the seismic incidence angle can significantly influence inelastic structural response. Studies on bidirectional excitation have shown that peak displacement, storey drift, ductility demand, and collapse-related indicators may vary appreciably with input orientation, especially for nonlinear systems, asymmetric buildings [9, 10]. In parallel, ground-motion component definitions have evolved substantially. Orientation-independent measures such as GMRotDpp, GMRotIpp, RotD50, and RotD100 were introduced to reduce the dependence of intensity measures on arbitrary sensor orientation and to provide consistent scalar definitions for ground-motion modeling and hazard analysis [11, 12]. These measures are essential for seismic hazard representation and record-selection procedures. However, they should not be confused with a complete solution to the input-orientation problem in NLTHA. A RotD100 spectral ordinate, for example, identifies the maximum oscillator response at a given period, but the orientation that maximizes the response may vary with period. Therefore, a maximum-direction response spectrum does not necessarily define a unique pair of time histories to be applied to a nonlinear three-dimensional building model.

The present study introduces a novel methodology termed Peak-Polar Rotation Intensity Ordinates, hereafter PP-RIO, which adopts a polar representation of ground motion directionality to statistically evaluate the input orientations associated with the most severe seismic demand for groups of earthquakes. This Intensity-based rotation framework is applied to an extensive dataset comprising more than 3400 FN and FP oriented earthquake recordings compiled from major international repositories, including NGA-West2 [13], K-NET and KiK-net [14], ESM [15], ITACA [16], and TADAS [17]. The proposed approach is not intended to replace hazard-consistent record selection or amplitude scaling. Rather, it addresses a subsequent and distinct step: the orientation of the selected horizontal record pair. The working hypothesis is that orientations associated with maximum PP-RIO, particularly cumulative energy-related measures such as Cumulative Absolute Velocity (CAV) and Specific Energy Density (SED), may provide a more stable proxy for high nonlinear demand than sensor axes, sparse fixed rotations, or fault-based orientations alone. This hypothesis is evaluated using far-field (FF), near-field non-pulse (NF), and pulse-like near-fault (PL) records applied to an eight-storey reinforced concrete frame model. Structural response is assessed through bidirectional demand quantities, including roof displacement and storey drift.

Accordingly, the practical implication examined in this work is whether a selected bidirectional record, when oriented according to a maximum-intensity direction, can reveal nonlinear deformation demands that are not captured by conventional fault-aligned or fixed-rotation protocols. PP-RIO is therefore framed as a complementary orientation check for NLTHA, rather than as a replacement for hazard-consistent record selection, amplitude scaling, or code-based orientation requirements. Within this scope, the paper makes three main contributions. First, it formulates a reproducible intensity-measure-based procedure for defining principal input orientations from the actual bidirectional time histories. Second, it quantifies, for the investigated eight-storey reinforced concrete frame, the changes in roof displacement and storey drift demand obtained from PP-RIO orientations relative to FN/FP and fixed-rotation alternatives. Third, it evaluates whether cumulative intensity measures, particularly CAV and SED, provide more stable orientation criteria than instantaneous peak measures such as PGA for the selected structural model and record subset. The study does not perform target-spectrum matching; it focuses on the orientation of already selected bidirectional records before their use in NLTHA.

The paper is structured to guide the reader from theoretical foundations to practical application. Section 2 provides a critical review of the state of the art, addressing limitations in current ground motion models and tracing the evolution of directionality modeling from dynamic analysis and probabilistic characterizations. Section 3 describes the seismotectonic framework and the ground motion datasets employed. Section 4 introduces the PP-RIO methodology. A statistical characterization of directionality features is presented in Section 5 to define the hazard input prior to structural application. Section 6 presents the reference eight-storey reinforced concrete building and the numerical modeling strategy. The main results are discussed in Section 7, focusing on Engineering Demand Parameters (EDP), followed by a comparative discussion of the PP-RIO methodology and conventional orientation protocols in Section 8. Finally, Section 9 summarizes the principal findings and outlines directions for future research.

10969845, 0, Downloaded from https://onlinelibrary.wiley.com/doi/10.1002/eqe.70286 by Marco Domaneschi - Politecnico Di Torino Sist. Bibl Del Polit Di Torino , Wiley Online Library on [26/08/2026]. See the Terms and Conditions (https://onlinelibrary.wiley.com/terms-and-conditions) on Wiley Online Library for rules of use; OA articles are governed by the applicable Creative Commons License

2 | Historical Perspectives and Advancements in Seismic Directionality

The seismic demand imposed on a structural system is governed not only by the amplitude, frequency content, and duration of the ground motion, but also by the orientation of the horizontal components with respect to the structural axes. In bidirectional nonlinear time-history analysis, two orthogonal acceleration time histories are applied simultaneously to the numerical model. This operation implicitly requires the selection of an incidence angle, even when that angle is not explicitly treated as an analysis variable [18]. Consequently, the adopted orientation of the input motion becomes part of the definition of the seismic action.

In conventional design procedures, the influence of directionality has often been addressed through simplified component-combination rules. Early developments in multicomponent seismic analysis focused on estimating critical responses in linear systems by combining modal or spectral responses associated with orthogonal horizontal components. Contributions by Wilson and Button [19] and Menun and Der Kiureghian [20] provided important formulations for considering the critical orientation of seismic input in linear response-spectrum analysis. These approaches remain useful in design contexts because they provide efficient estimates of directional demand without requiring direct integration of acceleration histories.

The problem becomes more complex in nonlinear dynamic analysis. Once yielding, stiffness degradation, strength deterioration, and geometric nonlinearity are activated, the structural response becomes path-dependent. The incidence angle may influence not only peak displacement or drift, but also the sequence of plastic hinge formation, the interaction between orthogonal resisting systems, torsional response, residual deformation, and local strain demand. Therefore, the critical orientation in NLTHA cannot be inferred solely from linear modal properties or from scalar spectral ordinates. It emerges from the interaction between the directional properties of the record and the nonlinear characteristics of the structure.

Several studies have shown that the angle of incidence can significantly affect inelastic demand. Rigato and Medina [18] investigated inelastic single-storey systems subjected to bidirectional ground motions and demonstrated that structural response may vary substantially with input orientation. Reyes and Kalkan [21], examined the implications of rotating ground motions to fault-normal/fault-parallel and maximum-direction orientations for response-history analysis of buildings, showing that different orientation protocols may lead to different estimates of engineering demand parameters. Kostinakis et al. [22], as well as Fontara et al. [23], further examined bidirectional excitation in reinforced concrete buildings, highlighting the dependence of directional sensitivity on structural configuration, inelastic response level, and ground-motion characteristics. Cantagallo et al. [24], showed that record selection and scaling procedures can also influence the observed directionality effects, while Skoulidou and Romão [9] emphasized the importance of considering multiple incidence angles when estimating seismic demand in nonlinear assessment.

These studies collectively indicate that input orientation is not a secondary modeling detail in bidirectional NLTHA. For some records and structural systems, the variation of response with incidence angle may be modest; for others, especially near-fault and pulse-like motions, directional amplification can be significant. This variability motivates the development of record-specific orientation procedures capable of identifying meaningful axes of ground-motion intensity before structural analysis is performed.

2.1 | Horizontal Component Definitions and Orientation-Independent Measures

The question of directionality has also been extensively studied from the standpoint of ground-motion intensity measures and ground-motion model development. Historically, many empirical models used scalar representations of the two horizontal components, frequently based on average or geometric-mean definitions. Although such measures are practical for hazard analysis and record selection, they reduce the two-dimensional horizontal motion to a single scalar quantity and therefore cannot fully describe the orientation-dependent distribution of shaking. To reduce the dependence of intensity measures on arbitrary sensor orientation, Boore, Watson-Lamprey, and Abrahamson introduced orientation-independent geometric-mean measures, including GMRotDpp and GMRotIpp [11]. These quantities are computed by rotating the two horizontal components over all non-redundant azimuths and evaluating percentile-based measures of the geometric mean.

Boore later introduced non-geometric-mean orientation-independent measures, commonly denoted as RotDnn, from which RotD50 and RotD100 are widely used. RotD50 represents a median horizontal spectral ordinate over rotation angles, whereas RotD100 represents the maximum spectral ordinate over rotation angles at a specified oscillator period [12]. These definitions have been fundamental for modern seismic hazard analysis, ground-motion model development, and the specification of design-compatible intensity measures. They provide a consistent way to describe horizontal ground motion independently of the arbitrary orientation of recording instruments. However, their role in nonlinear time-history analysis must be interpreted carefully. RotD50 and RotD100 are spectral component definitions; they describe the distribution of oscillator response over rotated horizontal components. They do not, by themselves, define the actual pair of orthogonal time histories to be applied to a nonlinear three-dimensional structural model.

This distinction is especially relevant for RotD100. The orientation that maximizes spectral acceleration is generally period-dependent. Therefore, a RotD100 spectrum does not necessarily correspond to a single physical rotation of the original accelerogram over the full period range of engineering interest. For nonlinear structures, where effective periods evolve during the response because of yielding and stiffness degradation, this limitation becomes more pronounced. Recent work by Rivera-Figueroa and Montejo [25], and by Rivera-Figueroa et al. [26], has further shown that the way in which records are made compatible

10969845, 0, Downloaded from https://onlinelibrary.wiley.com/doi/10.1002/eqe.70286 by Marco Domaneschi - Politecnico Di Torino Sist. Bibl Del Polit Di Torino , Wiley Online Library on [26/08/2026]. See the Terms and Conditions (https://onlinelibrary.wiley.com/terms-and-conditions) on Wiley Online Library for rules of use; OA articles are governed by the applicable Creative Commons License

with RotD100 targets can influence record characteristics and bidirectional inelastic response. These studies highlight the need to distinguish between spectral component definitions, target-spectrum compatibility, and the orientation of the time histories used in NLTHA. As depicted in subsequent sections, the present work follows this distinction. Orientation-independent spectral measures provide important background for understanding horizontal directionality, but the operational problem addressed here is different: given a selected bidirectional ground-motion pair, the aim is to identify an orientation of the actual time histories that is representative of strong directional intensity and then evaluate its consequences through NLTHA.

2.2 | Fault-Based Orientations and Polarized Near-Field Motions

When source-to-site geometry is known, the two horizontal components may be transformed from their original sensor axes into FN and FP components. This transformation provides a physically interpretable reference frame, particularly for near-fault motions affected by rupture directivity. Forward-directivity effects can generate coherent velocity pulses with a dominant polarization, often concentrated approximately in the FN direction. Such pulses may impose severe displacement and ductility demands on structures, especially when their characteristic pulse period is close to or longer than the initial fundamental period of the structure.

The destructive potential of pulse-like records is not simply a matter of harmonic resonance. Near-fault pulses typically involve one or a few large-amplitude cycles rather than sustained periodic excitation. Their effect on nonlinear systems is instead governed by the relationship between pulse period, structural period, and the period elongation that occurs after yielding. Studies by Alavi and Krawinkler [27], Champion and Liel [28], Roman-Velez and Montejo [29], and Montejo [30] have shown that severe inelastic displacement demand and reduced collapse capacity may occur when the pulse period exceeds the initial structural period, particularly within ranges where yielding-induced elongation brings the structure into stronger interaction with the pulse.

Although FN/FP axes are physically meaningful, they do not necessarily coincide with the orientation of maximum recorded intensity. Source complexity, rupture propagation, radiation pattern, basin effects, scattering, topographic amplification, and local site conditions may all modify the direction in which the strongest horizontal projection is observed at a station. Conversely, far-field records should not be interpreted as entirely non-polarized. While source-controlled directivity effects are generally less pronounced at larger distances, wave propagation through heterogeneous media, basin-edge effects, surface waves, and site-specific conditions may still produce directional features in the horizontal motion. For this reason, the classification of records into far-field, near-field non-pulse, and pulse-like regimes provides useful seismological context, but it does not remove the need to quantify the directional properties of each record. A record-specific description of polarization and intensity orientation is therefore required when the objective is to study how the horizontal wavefield interacts with structural axes in NLTHA.

2.3 | Principal Directions of Ground Motion Intensity

Several approaches have been proposed to identify principal directions of horizontal ground motion. Some are based on the geometry of the particle-motion trajectory; others use energy-related measures, covariance matrices, response spectra, or oscillator response. Hong and Goda [31] investigated horizontal ground-motion measures along principal directions and showed that the principal direction of an energy-type measure does not necessarily coincide with the major response axis defined by spectral acceleration at a given period. This distinction is important because different intensity measures emphasize different aspects of the same ground motion.

Peak Ground Acceleration identifies the orientation of the largest instantaneous acceleration projection. It is sensitive to short-duration, high-frequency peaks and may be relevant for acceleration-sensitive response quantities. Arias Intensity integrates the squared acceleration over the duration of the record and therefore reflects both amplitude and duration of shaking. Cumulative Absolute Velocity accumulates absolute acceleration over time and has been used as an indicator of potentially damaging motion. Specific Energy Density provides an energy-flux-related measure and is therefore naturally connected to cumulative input severity. These measures do not necessarily produce the same principal orientation, because they assign different weights to peak amplitude, frequency content, duration, and cumulative energy.

For nonlinear structural response, this distinction is relevant. Damage-sensitive response quantities are rarely controlled by a single instantaneous acceleration peak. They may depend instead on the cumulative deformation history, the number and amplitude of inelastic excursions, and the duration over which energy is transmitted to the structure. This provides the motivation for considering not only PGA-based orientations, but also orientations derived from integral measures such as Arias Intensity, CAV, and SED. Geometric descriptors of the horizontal trajectory can complement these intensity-based orientations. The envelope, ellipticity, or convexity of the polar trajectory provides information on whether the motion is nearly isotropic or strongly concentrated along a preferred direction. Similar concepts have appeared in recent work on directionality factors and RotD100-compatible records. In the present study, this type of geometric characterization is used to describe the directional concentration of the ground-motion dataset, while the input orientations adopted for NLTHA are defined through the maximization of selected scalar intensity measures.

2.4 | Motivation for an Intensity-Based Orientation Procedure

The literature reviewed above suggests that no single reference frame is universally sufficient for bidirectional nonlinear assessment. Sensor axes preserve the original recording orientation but are not generally related to the source, site, or structural system. Fault-normal and fault-parallel axes provide a physically meaningful description of near-fault rupture effects, but they do not necessarily define the maximum-intensity direction at a

10969845, 0, Downloaded from https://onlinelibrary.wiley.com/doi/10.1002/eqe.70286 by Marco Domaneschi - Politecnico Di Torino Sist. Bibl Del Polit Di Torino , Wiley Online Library on [26/08/2026]. See the Terms and Conditions (https://onlinelibrary.wiley.com/terms-and-conditions) on Wiley Online Library for rules of use; OA articles are governed by the applicable Creative Commons License

recording station. Fixed rotations provide additional samples of the directional response space, but their interpretation depends on the selected angles and they may miss demand-amplifying orientations.

An alternative is to define the orientation directly from the recorded bidirectional motion by rotating the horizontal pair over the non-redundant azimuthal domain and identifying the direction that maximizes a selected intensity measure. This approach preserves the original time histories, retains the orthogonal companion component, and provides a reproducible rule for defining the input axes prior to NLTHA. Its usefulness depends on whether the selected intensity measure identifies an orientation that is consistently associated with high nonlinear demand.

This is the context in which the Peak-Polar Rotation–Intensity Ordinates methodology is formulated. PP-RIO defines principal input orientations from the polar distribution of selected ground-motion intensity measures, including PGA, Arias Intensity, CAV, and SED. The method does not require modifying records to match a maximum-direction target spectrum. Instead, it acts on the selected bidirectional record pair by assigning a physically interpretable orientation to the actual accelerograms used in the nonlinear analysis.

The following sections develop this idea in two stages. First, the directional characteristics of a large set of far-field, near-field non-pulse, and pulse-like records are examined to identify regime-dependent patterns of polarization and intensity concentration. Second, selected records are applied to a nonlinear reinforced concrete frame model to evaluate how different orientation protocols affect engineering demand parameters. Through this sequence, the study connects ground-motion directionality with its structural responses in bidirectional NLTHA.

3 | Dataset Characterization and Seismotectonic Context

The ground motion database selected for this study comprises a comprehensive catalog of more than 3400 seismic records spanning approximately 70 years. The dataset was assembled from multiple strong motion repositories to ensure high-quality metadata availability, including key geophysical parameters such as the time-averaged shear-wave velocity in the top 30 meters (V_{s30}), local site classification, and precise hypocentral coordinates, and magnitudes over 4.5. A defining feature of this dataset is the preprocessing of the horizontal acceleration pairs. Unlike raw strong-motion repositories, which typically provide components in arbitrary geographic or sensor-based orientations, the recordings considered herein were systematically expressed in the FN/FP reference frame when the required fault geometry was available. This azimuthal consistency reduces the dependence of the analysis on random sensor orientation and provides a physically interpretable reference system.

The dataset is preclassified into three regimes based on source-to-site geometry and kinematic characteristics: Far-Field (FF), Near-Field non-pulse (NF), and Pulse-Like (PL). The identification of the PL subset was performed according to the quantitative wavelet-based procedure proposed by Baker [32]. In this approach, the velocity time history is decomposed using wavelet analysis to extract the dominant coherent velocity pulse. The classification is then based on the relative significance of the extracted pulse with respect to the original record, commonly expressed through pulse-related predictors such as the PGV ratio and energy ratio. Records with a sufficiently large pulse indicator are classified as pulse-like. The remaining near-source records that do not satisfy these pulse-like criteria are treated as NF records.

The global distribution of the selected events is illustrated in Figure 1. Epicenters are concentrated in major seismically active crustal regions, with significant clusters in the western United States, the Mediterranean basin (Italy, Turkey, and Greece), Japan, Taiwan, and New Zealand. This geographic diversity ensures that the dataset captures a broad spectrum of tectonic mechanisms, ranging from strike-slip faults in California and Turkey to subduction and thrust interfaces in Japan and Taiwan. Consequently, the statistical trends derived from this dataset are not site-specific artifacts but are representative of global active crustal seismicity.

The moment magnitude (M_w) distribution is presented in Figure 2a. The dataset provides robust sampling of moderate-to-strong earthquakes, with the modal range centered between M_w 6.0 and 6.5. FF ground motions numerically dominate the dataset, providing a statistically stable reference group representative of larger-distance recordings in which source-controlled near-fault polarization is generally less pronounced. In contrast, the PL subset reveals a distinct magnitude threshold: PL records are virtually absent below M_w 5.5. This observation is consistent with seismological theory, according to which coherent rupture directivity pulses require sufficient rupture length and energy release to generate long-period velocity pulses through constructive interference.

The spatial characteristics of the dataset are further examined through the epicentral distance (R_{epi}) distribution shown in Figure 2b. A clear classification boundary is defined at $R_{epi} = 20$ km. The NF and PL subsets are strictly confined to the near-source domain ($R_{epi} \leq 20$ km). The high density of short-distance records is particularly relevant for investigating near-fault effects, where ground motion is dominated by source characteristics rather than path attenuation. In contrast, FF records ($R_{epi} > 20$ km) exhibit a heavy-tailed distribution extending beyond 200 km. This broad range allows the analysis to examine the tendency toward reduced source-controlled polarization with increasing distance, while recognizing that scattering, multipathing, and local site effects may still generate directional features in individual FF records.

Finally, the scatter plot in Figure 3 correlates magnitude with logarithmic epicentral distance, providing a visual validation of the dataset coverage. Distinct clustering patterns highlight the hazard scenarios addressed in this study. In particular, the PL records form a dense cluster within the high-hazard domain defined by $M_w > 6.0$ and $R_{epi} < 15$ km. The absence of data gaps in this critical region supports reliable statistical inference in the subsequent directionality analyses.

10969845, 0, Downloaded from https://onlinelibrary.wiley.com/doi/10.1002/eqe.70286 by Marco Domaneschi - Politecnico Di Torino Sist. Bibl Del Polit Di Torino , Wiley Online Library on [26/08/2026]. See the Terms and Conditions (https://onlinelibrary.wiley.com/terms-and-conditions) on Wiley Online Library for rules of use; OA articles are governed by the applicable Creative Commons License

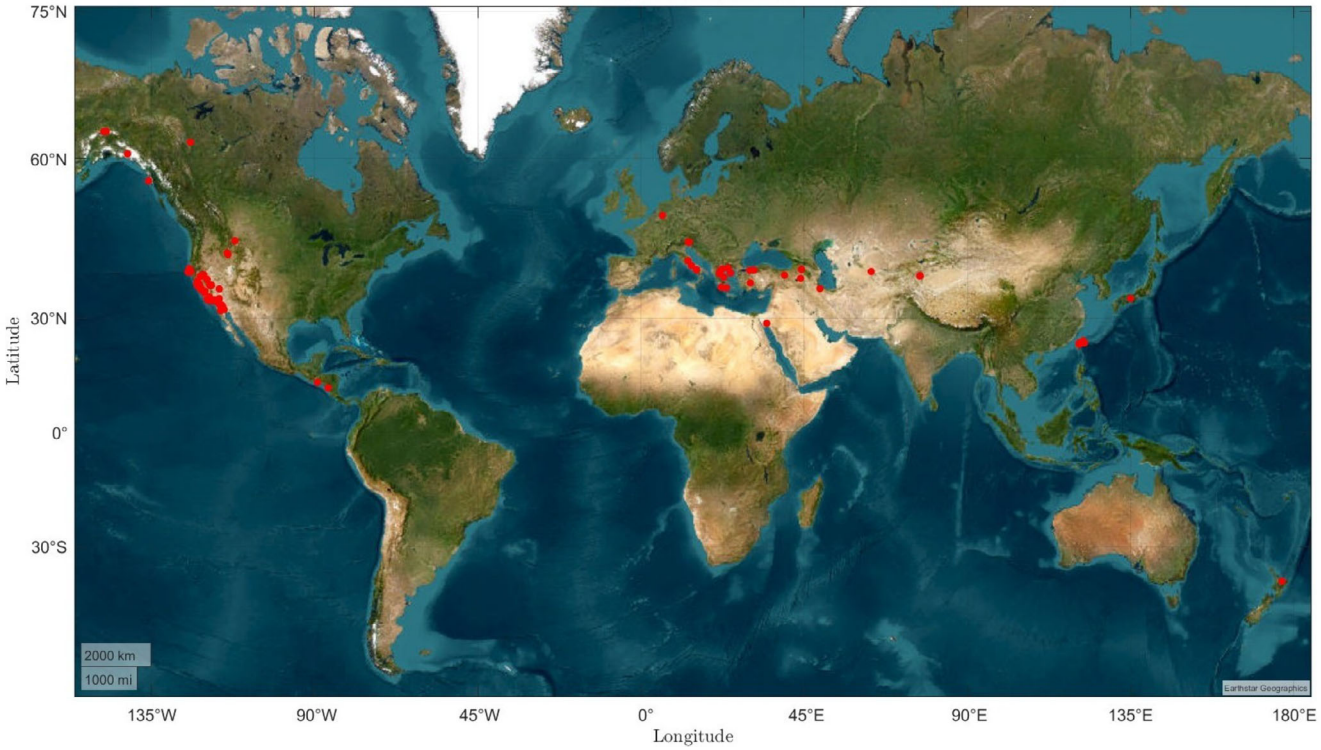

FIGURE 1 | Global distribution of epicenters, with clusters in the western U.S., the Mediterranean (Italy–Turkey–Greece), Japan, Taiwan, and New Zealand. This coverage spans major faulting mechanisms and plate-boundary settings, so the derived statistics are representative of global active crustal seismicity.

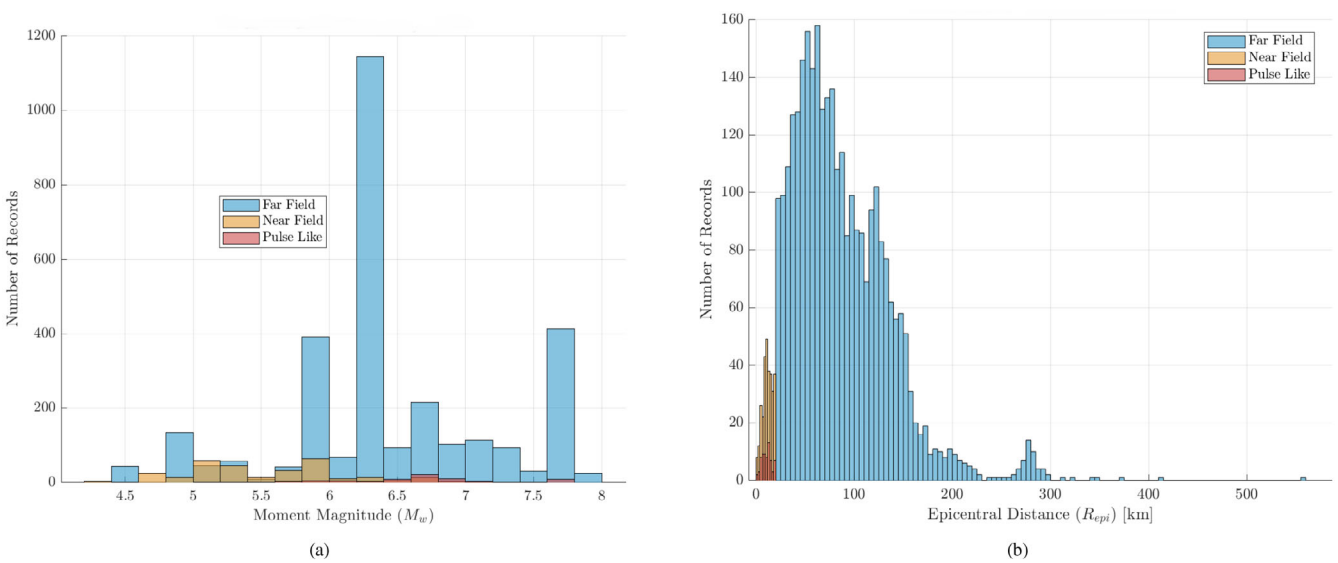

FIGURE 2 | Distribution of the selected records by class. (a) Moment magnitude (M_w) distribution of events contributing to the dataset. (b) Epicentral distance (R_{epi}, km) distribution of the recordings, showing the overall distance span and the relative contribution of far-field, near-field, and pulse-like subsets.

4 | Peak-Polar Rotation-Intensity Ordinates Method (PP-RIO)

The methodology proposed in this study, denoted as PP-RIO, establishes a deterministic approach for orienting bidirectional seismic recordings. Rather than prescribing the input axes from the original sensor azimuth, fault-aligned coordinates, or fixed geometric rotations, PP-RIO defines a record-specific reference frame from the direction that maximizes a selected scalar IM when performing NLTHA. By aligning the seismic input with the direction associated with the maximum polar IM, the PP-RIO method foresees that structural demand parameters are evaluated

10969845, 0, Downloaded from https://onlinelibrary.wiley.com/doi/10.1002/eqe.70286 by Marco Domaneschi - Politecnico Di Torino Sist. Bibl Del Polit Di Torino , Wiley Online Library on [26/08/2026]. See the Terms and Conditions (https://onlinelibrary.wiley.com/terms-and-conditions) on Wiley Online Library for rules of use; OA articles are governed by the applicable Creative Commons License

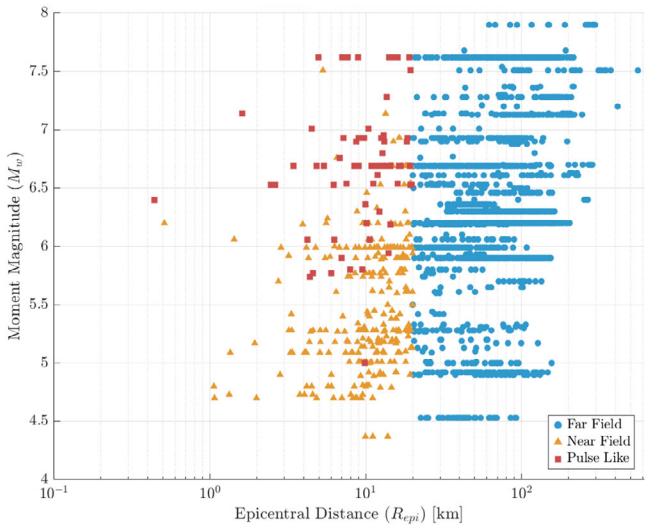

FIGURE 3 | Magnitude–distance distribution of the selected ground motions. Moment magnitude (M_w) is plotted against epicentral distance (R_{epi}, km; log-scale), with markers distinguishing FF, NF, and PL records, highlighting the complementary coverage of the dataset across source size and recording distance.

against the most critical loading vector physically present in the ground motion history. The procedural workflow is illustrated in Figure 4 and defined in the following subsections.

4.1 | Phase 1: Signal Preprocessing–Trimming

The horizontal accelerometric records are first subjected to a standard preprocessing sequence, including baseline correction and band-pass filtering, in order to reduce low-frequency drift and high-frequency noise associated with triggering, instrumental effects, and ambient vibration. Although Phase 1 of Figure 4 illustrates this operation for a single horizontal component for graphical clarity, the trimming procedure is defined from the combined bidirectional motion. Therefore, the same time window is subsequently applied to both orthogonal components, preserving their temporal synchronization and relative phase.

To this end, the two horizontal components, here denoted as $a_{FP}(t)$ and $a_{FN}(t)$, are combined in polar form. The instantaneous horizontal acceleration vector $\mathbf{R}(t)$ is described by its polar magnitude $R_o(t)$ and phase angle $\theta(t)$ as

$$R_o(t) = \sqrt{a_{FN}(t)^2 + a_{FP}(t)^2}, \tag{1}$$

$$\theta(t) = \text{atan2}\,(a_{FN}(t), a_{FP}(t)), \tag{2}$$

where the use of the four-quadrant function atan2(·) preserves the correct azimuthal position of the instantaneous acceleration vector in the horizontal plane.

The effective strong-motion window is identified from the polar resultant rather than from either component separately. In the PGA-based implementation illustrated in Figure 4, the reference instant is obtained from the maximum polar acceleration,

$$PGA_{\text{pol}} = \max_t\,[R_o(t)], \qquad t_p = \arg\max_t\,[R_o(t)], \tag{3}$$

and the corresponding phase angle is defined as

$$\theta_p = \theta(t_p). \tag{4}$$

Thus, θ_p represents the orientation of the maximum instantaneous horizontal acceleration vector, while PGA_{pol} provides the reference amplitude for the subsequent normalization. The trimming window shown in Phase 1 is therefore centered on, or otherwise defined with respect to, the strong-motion interval containing t_p, and is then imposed consistently on both horizontal components. This ensures that the signal segment used in the following phases is governed by the maximum bidirectional intensity of the record rather than by a peak occurring in only one component.

The resulting preprocessed and synchronized pair constitutes the input for the deterministic rotation in Phase 2, where the reference axes are aligned with the principal polar direction θ_p.

4.2 | Phase 2: Deterministic Rotation; Principal IM Direction

To standardize the directional reference system prior to the geometric characterization, the bidirectional record is rigidly rotated by the principal angle θ_p identified in the previous step. This transformation aligns the direction of the maximum polar Intensity Measure vector, PGA_{pol} for this specific application, with the reference axis of the rotated coordinate system. The original pair $(a_{FP}(t), a_{FN}(t))$ is therefore transformed into a principal component, $a_P(t)$, and an orthogonal companion component, $a_O(t)$, as

$$\begin{bmatrix} N_{IM_{Principal}} \\ E_{IM_{Principal}} \end{bmatrix} = \begin{bmatrix} \cos\theta_p & \sin\theta_p \\ -\sin\theta_p & \cos\theta_p \end{bmatrix} \begin{bmatrix} a_{FN}(t) \\ a_{FP}(t) \end{bmatrix}. \tag{5}$$

In this rotated frame, the principal component contains the maximum polar intensity measure observed during the record, while the orthogonal component preserves the bidirectional character of the excitation. Hence, the procedure does not discard any horizontal component of the motion; it only redefines the reference axes according to the record-specific direction of maximum intensity. This differs from fixed-angle rotations, where the incidence angles are prescribed independently of the ground-motion trajectory.

The rotated components are subsequently normalized by the maximum intensity measure, herein PGA_{pol}, so that the maximum polar radius of the normalized trajectory is equal to unity. This normalization preserves the shape and directional distribution of the acceleration trajectory, while allowing records with different amplitudes to be compared in a common nondimensional polar domain.

As illustrated in Phase 2 of Figure 4, a Kernel Density Estimation (KDE) is introduced at this stage as an explanatory diagnostic of

10969845, 0, Downloaded from https://onlinelibrary.wiley.com/doi/10.1002/eqe.70286 by Marco Domaneschi - Politecnico Di Torino Sist. Bibl Del Polit Di Torino , Wiley Online Library on [26/08/2026]. See the Terms and Conditions (https://onlinelibrary.wiley.com/terms-and-conditions) on Wiley Online Library for rules of use; OA articles are governed by the applicable Creative Commons License

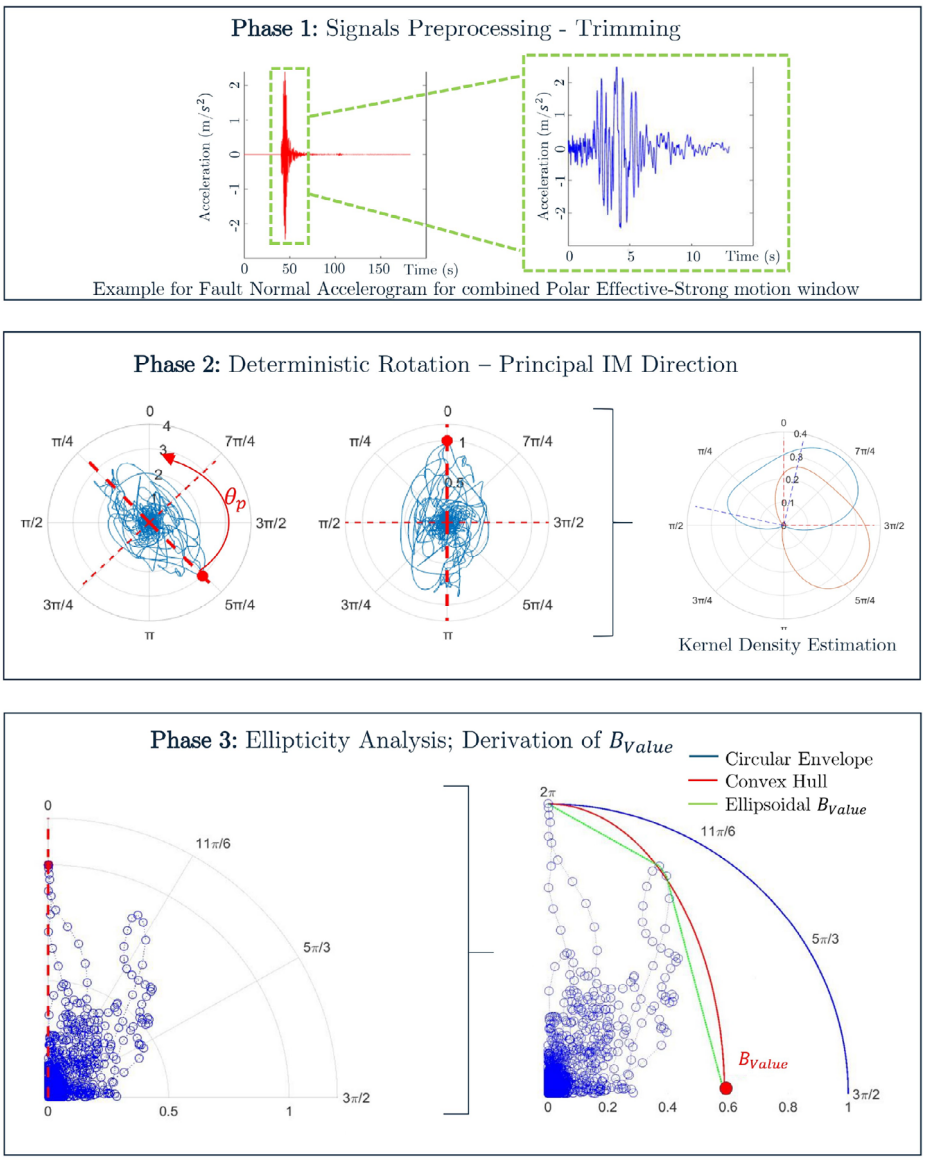

FIGURE 4 | Workflow of the PP-RIO procedure for identifying the polar principal orientation and deriving the b_{Value} polarization descriptor. Phase 1 shows the preprocessing and trimming of the accelerometric signal. Although one horizontal component is illustrated for clarity, the effective strong-motion window is defined from the combined polar resultant of the two synchronized horizontal components and is then applied consistently to both records. Phase 2 presents the deterministic rotation of the bidirectional acceleration trajectory toward the principal IM direction, defined by the angle θ_p associated with the maximum polar intensity. The Kernel Density Estimation is included only as an illustrative diagnostic to visualize the directional concentration of the rotated samples in polar space. Phase 3 shows the normalized and folded polar trajectory used for the ellipticity analysis. The convex hull defines the outer directional support of the acceleration point cloud, while the fitted ellipsoidal envelope provides the scalar descriptor b_{Value}. Lower b_{Value} values indicate stronger polarization and a more elongated trajectory, whereas values approaching unity indicate a more isotropic distribution of horizontal intensity.

the rotated polar trajectory. The KDE is not used as a record-by-record processing operation and does not enter the calculation of either θ_p or b_{Value}. Its role is to show, for the representative record used in the flowchart, how the acceleration samples concentrate after the deterministic alignment. This is useful because the raw polar trajectory may appear visually scattered, whereas the KDE highlights the dominant directional density of the motion and inspired the transition toward the quadrant-folded representation adopted in Phase 3.

Therefore, Phase 2 performs two distinct functions: first, it defines an intensity-aligned reference frame through the deterministic rotation by θ_p; second, it uses KDE only as a visual analysis to understand the concentration of the normalized acceleration samples, subsequently inspiring the implementation of a convex-hull algorithm and elliptic-envelope characterization.

4.3 | Phase 3: Ellipticity Analysis; Derivation of B_{Value}

While the procedure previously introduced identifies the peak demand, characterizing the global directionality requires analyzing the full distribution of the acceleration trajectory in polar

10969845, 0, Downloaded from https://onlinelibrary.wiley.com/doi/10.1002/eqe.70286 by Marco Domaneschi - Politecnico Di Torino Sist. Bibl Del Polit Di Torino , Wiley Online Library on [26/08/2026]. See the Terms and Conditions (https://onlinelibrary.wiley.com/terms-and-conditions) on Wiley Online Library for rules of use; OA articles are governed by the applicable Creative Commons License

space. As depicted in the Phase 3 of Figure 4, this is achieved through a geometric fitting algorithm:

1. **Normalization and Quadrant Folding**: The polar magnitude $R_o(t)$ is normalized by PGA_{pol} such that the maximum radius is unity ($r_{max} = 1$). To facilitate envelope fitting, the absolute values of the trajectory are folded into the first quadrant ($0 \leq \theta \leq \pi/2$), mapping the bidirectional energy distribution into a bounded domain.
2. **Convex Hull Determination**: The outer directional support of the normalized acceleration trajectory is extracted by computing the Convex Hull of the folded point cloud, shown by the green boundary in Phase 3 of Figure 4. The convex hull defines the minimum convex polygon enclosing all normalized samples and therefore provides the smallest geometric envelope of the observed bidirectional motion in polar space. Physically, this operation isolates the extreme directional content of the record from the dense low-amplitude region of the trajectory. It is therefore well suited to characterize the directional spread of the strong-motion trajectory.
3. **Elliptical Optimization**: An optimization algorithm fits a geometrical envelope to the convex hull, later to be derived as an ellipse. The shape of this ellipse is governed by the semi-minor axis parameter, b, while the semi-major axis a is fixed at unity (representing the normalized peak). The governing polar equation for the elliptical boundary is derived as:

$$r(b, \theta) = \frac{b}{\sqrt{(b\cos\theta)^2 + (\sin\theta)^2}} \tag{6}$$

The optimal parameter resulting from this fit, denoted as b_{Value}, serves as a dimensionless index of polarization (see Phase 3 (right) Figure 4):

- $b_{Value} \to 0$: Highly polarized, near-linear motion (e.g., strong NF directivity pulses).
- $b_{Value} \to 1$: Isotropic, circular motion (typical of FF scattering).

This geometric characterization provides a continuous, quantitative metric of directionality, allowing for the sub-categorization of seismic events based on their kinematic radiation patterns rather than simple geographic proximity.

It is worth noting the use of a polar envelope to quantify directional concentration follows the same general rationale as previous area-based directionality measures developed for spectral response quantities [25]. In the present implementation, however, the envelope is constructed from the time-domain ground-motion trajectory after rotation and normalization. The resulting b_{Value} is therefore interpreted as a kinematic polarization descriptor of the input record, not as a spectral directionality factor. It is used to characterize the directional concentration of the motion, whereas the PP-RIO incidence angle used in the NLTHA is obtained from the maximization of the selected scalar intensity measure.

5 | Statistical Analysis of Ground Motion Directionality

The geometric characterization of the dataset, quantified via the envelope ellipticity parameter B_{Value} introduced in Section 4, reveals distinct statistical signatures governing the directional nature of ground motion. By analyzing the dependency of B_{Value} on key seismological predictors, specifically moment magnitude (M_w) and epicentral distance (R_{epi}), the effects of source rupture dynamics can be decoupled from path-dependent wave propagation mechanisms.

5.1 | Isotropic Wavefield and Source Scaling

The evolution of polarization as a function of both propagation distance and source scaling is analyzed in Figure 5. Although the independent variable is Moment Magnitude (M_w), a distinct vertical stratification between the distance-based regimes has been observed across the entire magnitude spectrum. The Far-Field (FF) dataset, representing wavefields that have propagated over greater distances, consistently exhibits higher mean b_{Value} trajectories ascending toward 0.80. Conversely, the near-source regimes, comprising Near-Field (NF) and Pulse-Like (PL) records, maintain lower mean b_{Value} ranges. This recurrent vertical gap aligns with the Well-supported hypothesis of isotropization for the seismic wavefield. Regardless of the initial energy release, as the seismic wave train propagates into the far-field regions, scattering and multipathing effects caused by crustal heterogeneities degrade the phase coherence between orthogonal components. This scattering randomizes the particle motion, gradually transitioning from the initial source polarization and producing the isotropic energy distribution characteristic of FF records [33, 34].

Building upon this distance-based isotropization, the dependence of the polarization parameter b_{Value} on M_w further clarifies regime-specific directionality. The scatter data are segregated into PL, NF, and FF fields to reveal distinct dispersion patterns. Within the FF dataset (blue trend), a stable and slightly increasing b_{Value} across the magnitude spectrum is appreciated. This suggests that for distant sites, the source size (M_w) plays a secondary role relative to path effects; the wavefield is sufficiently randomized by attenuation mechanisms regardless of the initial earthquake size.

For PL events, a marked divergence is observed (red trend) at high magnitudes ($M_w > 7.0$). While moderate events show variable polarization, large-magnitude PL events exhibit a pronounced reduction in b_{Value}, dropping to $\mu \approx 0.67$ in the highest bin, compared to $\mu \approx 0.78$ for non-pulse NF records of comparable magnitude.

This finding is physically consistent with forward-directivity mechanics [35]. High-magnitude events involve longer rupture dimensions, which facilitates the constructive interference of the shear-wave front. This mechanism generates long-period, high-energy velocity pulses that are strongly polarized in the FN direction. The statistical evidence therefore confirms that extreme polarization is not solely a function of physical proximity,

10969845, 0, Downloaded from https://onlinelibrary.wiley.com/doi/10.1002/eqe.70286 by Marco Domaneschi - Politecnico Di Torino Sist. Bibl Del Polit Di Torino , Wiley Online Library on [26/08/2026]. See the Terms and Conditions (https://onlinelibrary.wiley.com/terms-and-conditions) on Wiley Online Library for rules of use; OA articles are governed by the applicable Creative Commons License

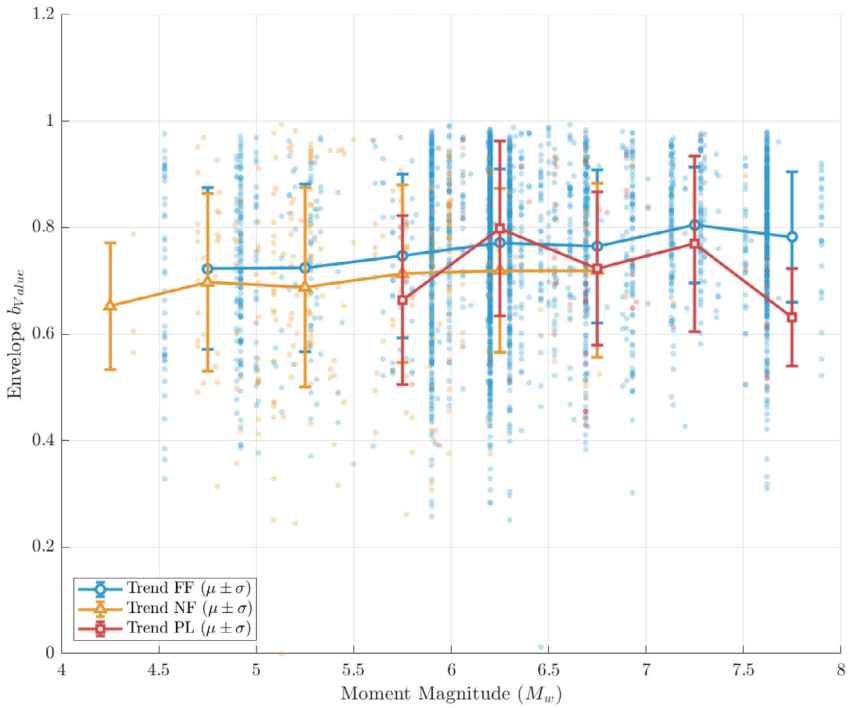

FIGURE 5 | Scatter and trend analysis of the envelope ellipticity descriptor b_{Value} as a function of moment magnitude (M_w) for the FF, NF, and PL subsets. Individual points represent single records, while connected markers indicate the mean b_{Value} computed within each magnitude bin. Error bars denote $\mu \pm \sigma$, where μ and σ are the mean and STD of b_{Value} within the corresponding bin.

but is highly amplified by coherent rupture dynamics in large earthquakes [36].

5.2 | Global Distribution and Regime-Dependent Polarization

The statistical distribution of b_{Value} across the three identified regimes is summarized in Figure 6. The box limits denote the first and third quartiles, the horizontal line indicates the median, the whiskers represent the lower and upper non-outlier ranges, and the red cross denotes the mean value. Since $b_{Value} \to 0$ represents a strongly polarized, nearly linear trajectory, whereas $b_{Value} \to 1$ corresponds to a more isotropic, nearly circular envelope, the figure provides a compact statistical description of the directional concentration of the horizontal acceleration field.

The FF subset exhibits the largest central tendency, with $\mu = 0.77$ and $\sigma = 0.14$. Its median and interquartile range are shifted toward higher b_{Value} values, indicating that FF records tend to mobilize comparable acceleration amplitudes over a broader range of horizontal orientations. In geometric terms, their normalized polar envelopes are more frequently close to circular, reducing the distinction between principal and secondary directions. Nevertheless, the lower whisker extends to values close to $b_{Value} \approx 0.4$, confirming that polarization is not exclusive to near-fault records and may also arise in some FF motions.

The NF and PL subsets exhibit lower mean values, $\mu = 0.70$ and $\mu = 0.71$, respectively, suggesting a stronger tendency toward directional concentration. Their distributions are shifted toward lower b_{Value} levels and show greater dispersion, particularly for NF records, for which $\sigma = 0.17$. This indicates that near-source motions do not present a unique polarization level, but rather include both moderately isotropic and strongly polarized records.

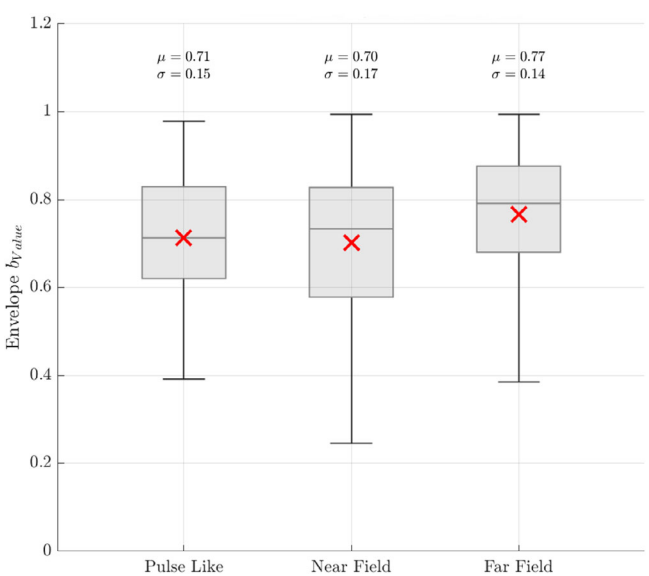

FIGURE 6 | Global statistical comparison of the envelope ellipticity descriptor b_{Value} across the PL, NF, and FF subsets. The box limits represent the first and third quartiles, the horizontal line inside each box denotes the median, the whiskers indicate the lower and upper non-outlier ranges, and the red cross marks the mean value. Lower b_{Value} values correspond to more elongated and directionally concentrated polar envelopes, whereas values approaching unity indicate a more isotropic distribution of horizontal intensity.

10969845, 0, Downloaded from https://onlinelibrary.wiley.com/doi/10.1002/eqe.70286 by Marco Domaneschi - Politecnico Di Torino Sist. Bibl Del Polit Di Torino , Wiley Online Library on [26/08/2026]. See the Terms and Conditions (https://onlinelibrary.wiley.com/terms-and-conditions) on Wiley Online Library for rules of use; OA articles are governed by the applicable Creative Commons License

The PL subset shows a central tendency comparable to the NF subset, although with slightly lower dispersion, consistent with the presence of coherent directional features associated with pulse-like near-fault motions. However, the overlap among the boxes and whiskers indicates that these trends should be interpreted statistically, not as deterministic regime separations.

Overall, Figure 6 shows that FF, NF, and PL records exhibit overlapping but distinguishable tendencies in terms of horizontal polarization. FF motions generally present higher ellipticity and weaker directional preference, whereas NF and PL records tend toward lower b_{Value} values and stronger directional concentration. Therefore, b_{Value} is not used as a categorical classifier of ground-motion regime, but as a continuous kinematic descriptor of polarization intensity that complements the seismological classification.

Within the PP-RIO framework, this descriptor also provides an additional directionality-based criterion for filtering and selecting accelerograms prior to structural analysis. b_{Value} quantifies the directional concentration of the horizontal acceleration trajectory itself. Records with low b_{Value} values exhibit a more elongated polar envelope and are therefore expected to be more sensitive to input orientation, whereas records with high b_{Value} values tend to show a more isotropic distribution of horizontal intensity. In this sense, b_{Value} is introduced as a complementary screening parameter, useful for identifying records whose polar characteristics are more likely to produce orientation-sensitive nonlinear structural response.

Finally, the PP-RIO framework presented in Section 4 is not restricted to the PGA-based orientation used to introduce the geometric analysis. The same polar-rotation procedure can be applied to alternative scalar IMs, allowing the principal direction to be defined according to different physical attributes of the ground motion. PGA emphasizes the maximum instantaneous acceleration projection, whereas Arias Intensity, Cumulative Absolute Velocity, and Specific Energy Density incorporate duration and cumulative energy-related effects. The influence of these alternative IM-based orientations on the nonlinear structural response is examined in the following sections.

6 | Structural Application: Numerical Modeling and Parametric Definition

The investigation focuses on an eight-storey reinforced concrete frame building, selected as representative of existing structures designed according to the former Italian seismic code DM96. The building is adopted from a published study in which its behavior under bidirectional loading was examined [37]. The structure is characterized by a rectangular multi-bay plan configuration measuring 28 × 18 m and a total height of 28 m (see Figure 7). Regarding the cross-sectional geometry, the structural system features primary column dimensions of 0.90 × 0.45 m, 0.50 × 0.50 m, and 0.50 × 0.35 m at the base levels (floors 1–4). These sections are reduced to 0.40 × 0.40 m and 0.45 × 0.30 *m* from the fifth level to the roof. The horizontal framing consists of interior beams measuring 0.80 × 0.24 m and 1.00 × 0.24 m, while the perimeter beams are dimensioned at 0.30 × 0.60 m).

Numerical simulations have been performed using OpenSees, the Open System for Earthquake Engineering Simulation [38], employing a distributed plasticity approach. The structural members are modeled via flexibility-based nonlinear beam-column elements with fiber sections, while geometric nonlinearities have been accounted for through P-Delta transformations [39, 40]. Inertial properties have been defined by concentrating masses at the nodal points, coupled with rigid diaphragm constraints to simulate floor stiffness. The applied gravitational loading includes structural self-weight (e.g., slab self-weight of 3.75 kN/m^2, non-structural components - partitions, flooring, and ceilings), and a residential live load of 2.00 kN/m^2. A damping ratio of 5%, proportional to both mass and tangent stiffness, has been assigned to the model [10, 37].

Following the application of gravity loads, the dynamic characteristics of the structure were evaluated. The building exhibits fundamental periods of $T_1 = 2.47$ s, $T_2 = 1.81$ s, and $T_3 = 1.69$ s. As expected, modal analysis reveals that the dynamic behavior is defined by two translational modes along the principal plan axes (Y and X) and a third torsional mode. To rigorously assess the influence of ground motion directionality, two Engineering Demand Parameters (EDP) have been selected: the maximum roof horizontal displacement (U) and the distribution of Storey Drift Ratio (SDR) along the height. The SDR is computed at each time step as the ratio of the vector magnitude of the relative displacement to the storey height.

To address the bidirectionality of cumulative damage potential, the PP-RIO methodology has been extended to integral-based IM, specifically *Arias Intensity (AI)* [41], *Cumulative Absolute Velocity (CAV)* [42], and *Specific Energy Density (SED)* [43]. As visualized in Figure 8, the procedure transcends the limitations of arbitrary sensor orientation (Case A) by performing a continuous coordinate transformation of the recorded orthogonal components, across the azimuthal domain. Through this rotation, the specific incidence angle corresponding to the maximization of the selected scalar IM is identified, defining the principal intensity axes (Case B). Unlike fixed geometric rotation schemes (Cases C and D) or unrotated recording orientations, this approach ensures that the numerical model is subjected to the maximum energy flux or cumulative demand inherent in the wavefield. Consequently, the input ground motions applied to the structural principal axes represent a physically realistic, cumulative intensity-based scenario for energy dissipation and damage accumulation, independent of the aleatory uncertainty associated with the original seismometer alignment.

7 | Analysis of Engineering Demand Parameters (EDPs)

To quantify the influence of ground-motion directionality on structural response, a series of NLTHA were performed for the three seismological datasets previously characterized: FF, NF, and PL. The response assessment is based on two primary Engineering Demand Parameters (EDPs): the Maximum Storey Drift Ratio (SDR) and the maximum roof displacement (U). These quantities are adopted as global deformation-based indicators, with SDR describing the distribution of storey deformation

10969845, 0, Downloaded from https://onlinelibrary.wiley.com/doi/10.1002/eqe.70286 by Marco Domaneschi - Politecnico Di Torino Sist. Bibl Del Polit Di Torino , Wiley Online Library on [26/08/2026]. See the Terms and Conditions (https://onlinelibrary.wiley.com/terms-and-conditions) on Wiley Online Library for rules of use; OA articles are governed by the applicable Creative Commons License

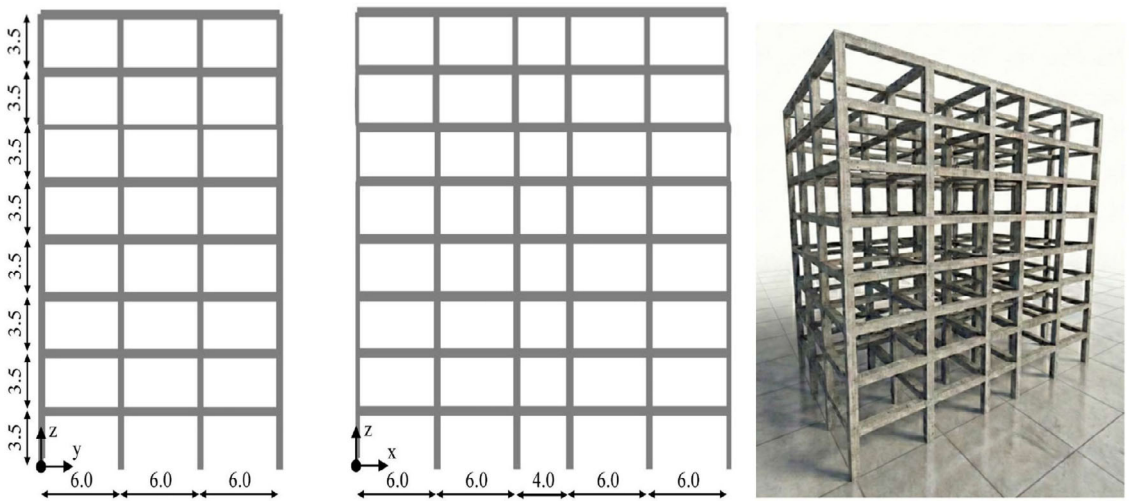

FIGURE 7 | Elevation views of the building structure. *Y-Y* axis elevation (left) and *X-X* axis elevation (center) and 3D isometric view of the structural frame (right).

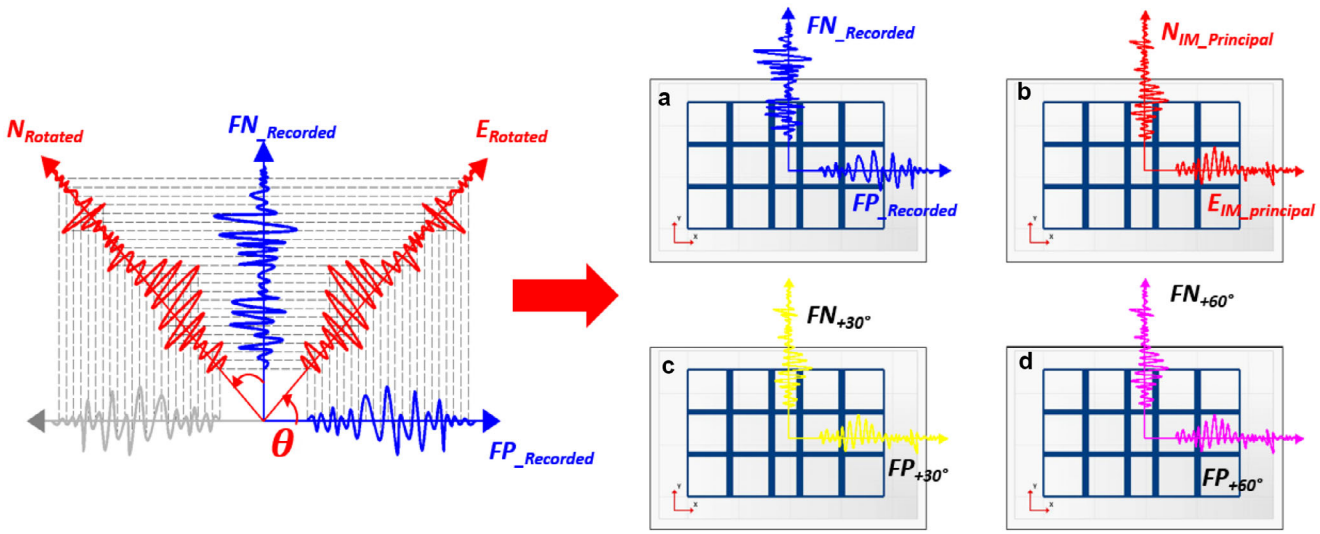

FIGURE 8 | Schematic representation of the PP-RIO methodology. The left panel depicts the continuous coordinate transformation of the fault-aligned orthogonal components ($FN_{Recorded}$, $FP_{Recorded}$) to identify the critical incidence angle θ that maximizes a selected IM. The right panels illustrate the comparative application strategies: (a) the original fault-aligned orientation relative to the structural plan; (b) the proposed methodology, wherein the structural axes are rigorously aligned with the principal intensity axes ($N_{IM_Principal}$, $E_{IM_Principal}$) corresponding to the maximum demand; and (c, d) conventional arbitrary rotation schemes (e.g., 30° and 60°).

along the building height and U representing the overall lateral displacement demand of the structural system.

The adopted numerical model includes both material and geometric nonlinearities; therefore, the computed response inherently reflects the evolution of inelastic behavior during the dynamic analyses. Within this framework, *SDR* and U are retained as the principal EDPs because they are widely used in seismic assessment and provide a consistent basis for comparing alternative input-orientation protocols. It is recognized that these quantities do not, by themselves, uniquely characterize local damage mechanisms, such as reinforcement strain, curvature ductility, or direction-dependent yield deformation. Nevertheless, when obtained from nonlinear response-history analyses, they provide a good global and storey-level measures of deformation severity and practical indicators of the relative inelastic demand induced by different ground-motion orientations.

The full database described in Section 5 was used for the statistical characterization of ground-motion directionality and polarization features. The subsequent NLTHA campaign was performed on a reduced and balanced subset of 45 records, comprising 15 FF, 15 NF, and 15 PL motions. This subset was defined prior to the structural analyses in order to keep the computational demand of the fiber-based nonlinear model tractable while preserving a comparable number of records in each seismological regime. Within each class, records were selected by prioritizing strong events, higher intensity levels, and lower b_{Value} values, so that the

10969845, 0, Downloaded from https://onlinelibrary.wiley.com/doi/10.1002/eqe.70286 by Marco Domaneschi - Politecnico Di Torino Sist. Bibl Del Polit Di Torino , Wiley Online Library on [26/08/2026]. See the Terms and Conditions (https://onlinelibrary.wiley.com/terms-and-conditions) on Wiley Online Library for rules of use; OA articles are governed by the applicable Creative Commons License

structural analyses would focus on motions with greater potential to produce orientation-sensitive nonlinear response, as the PP-RIO methodology is proposing. The use of the same number of records per regime also prevents the numerically dominant FF dataset from controlling the comparison and allows the response trends of FF, NF, and PL motions to be evaluated on a balanced basis. Accordingly, the record numbering used in the subsequent figures should be interpreted as a categorical identifier within each regime, not as a continuous physical variable.

For each selected record, the numerical model was subjected to fifteen distinct input-orientation protocols. These include the baseline fault-aligned condition, defined by the Fault-Normal/Fault-Parallel pair (FN/FP), two fixed geometric rotations of this pair by 30° and 60°, and four intensity-based orientations derived through the PP-RIO methodology, each also examined in its principal configuration and after additional rotations of 30° and 60°. The PP-RIO orientations correspond to the maximization of distinct scalar IMs: Peak Ground Acceleration (*PP-RIO Max*), Arias Intensity (*PP-RIO AI*), Cumulative Absolute Velocity (*PP-RIO CAV*), and Specific Energy Density (*PP-RIO SED*). This design of analyses enables a direct record-by-record comparison between conventional fault-aligned or fixed-rotation configurations and the proposed intensity-based orientations.

The selection of the 30° and 60° rotations was informed by preliminary incidence-angle sensitivity analyses performed during the initial stage of the study. In those analyses, representative records were rotated over the horizontal plane using 10° increments, starting both from the FN/FP reference system and from the PP-RIO-derived principal orientations. These preliminary analyses were used to evaluate the variability of the nonlinear response with respect to changes in incidence angle and to define a computationally tractable angular sampling strategy for the complete NLTHA campaign. The adopted 30° and 60° rotations therefore provide a structured benchmark of directional variability around each reference orientation, rather than a single arbitrary comparison angle.

The immediate analytical focus has been directed toward the PL regime. This prioritization is grounded in the statistical findings of the preceding Section 5, where the b_{Value} analysis demonstrated that PL events exhibit the most pronounced directional polarization. While the FF and non-pulse NF datasets, which exhibit stronger tendencies toward isotropy, remain integral to the overall validation, their performance implications are addressed in subsequent discussion sections.

To illustrate the applicative effects of incidence-angle assumptions for a PL event on the structural demand, the response history of the building subjected to a representative PL ground motion (Record ID 034) has been analyzed. This specific event is characterized by a NF velocity pulse, rendering the structural response highly sensitive to the alignment between the pulse azimuth, that is, the governing directionality, and the principal structural axes.

In the following illustrative results, the reported X-direction response corresponds to the structural axis intentionally aligned with the PP-RIO principal intensity direction. Accordingly, these quantities should be interpreted as critical-axis demands associated with the imposed input orientation, rather than as arbitrary single-component outputs from a bidirectional analysis. The orthogonal component of the response was retained and monitored throughout the analyses to verify that the principal-axis interpretation was not contradicted by a larger transverse demand.

7.1 | Applicative Effects, Top-Floor Displacement Demand Parameter

The time history evolution of the X-direction top floor displacement is presented in Figure 9. A significant dispersion in peak demand is observed across the considered reference systems. As evidenced in the displacement history, the standard fault-aligned orientation (FN/FP) yields a peak demand of only 0.148 m. However, this value is demonstrated to be non-conservative when compared to Intensity-based rotations. Specifically, orientations derived from IMs such as *Max*, *CAV* and *AI* identify critical directions that amplify the displacement demand to 0.314 m and 0.313 m, respectively. This corresponds to an amplification factor greater than 2.0 compared to the standard recording. It is noteworthy that fixed geometric rotations for the FN/FP orientation, such as *FN/FP rot.30* and *FN/FP rot.60*, exhibit inconsistent performance, with peaks of −0.24 m and +0.303 m, respectively. While they exceed the fault-aligned baseline, they fail to consistently capture the maximum demand envelope identified by the integral-based optimal orientations. The 60° rotation case relative to the FN/FP reference system happens to approach the effective principal direction; however, this proximity highlights the essentially arbitrary nature of a fixed-rotation approach.

7.2 | Applicative Effects, Storey Drift Demand Parameter

The previously presented implications of the PP-RIO principal direction on local damage potential are further highlighted in the storey-drift profiles shown in Figure 10. In this plot, the ordinate at each floor represents the maximum recorded storey drift attained at any time during the response history, thereby summarizing peak storey deformation demand along the height. The results indicate ductility demand across different reference systems. In particular, the standard fault-aligned orientation (*FN/FP*) suggests a maximum drift of approximately 3.9% concentrated around the 5th and 6th storeys. In contrast, the Intensity-based protocols (SED, CAV, and Max) shift the critical mechanism to the 4th storey and increase the maximum drift substantially to approximately 7.0%. This represents a near-doubling of the local ductility demand that is entirely neglected by the standard FN/FP. Furthermore, the storey drift profile highlights the volatility of arbitrary geometric rotations in PL regimes. While fixed rotations from the fault-aligned FN/FP such as *FN/FP* rot.30 and *FN/FP* rot.60 generate intermediate demands (approximately 5.5% and 4.5% respectively), they effectively function as an arbitrary selection exceeding the fault-aligned baseline but failing to capture the true worst case scenario. Consequently, the PP-RIO methodology, particularly when utilizing SED and CAV, offers a stable and intensity-aligned upper-bound estimate

10969845, 0, Downloaded from https://onlinelibrary.wiley.com/doi/10.1002/eqe.70286 by Marco Domaneschi - Politecnico Di Torino Sist. Bibl Del Polit Di Torino , Wiley Online Library on [26/08/2026]. See the Terms and Conditions (https://onlinelibrary.wiley.com/terms-and-conditions) on Wiley Online Library for rules of use; OA articles are governed by the applicable Creative Commons License

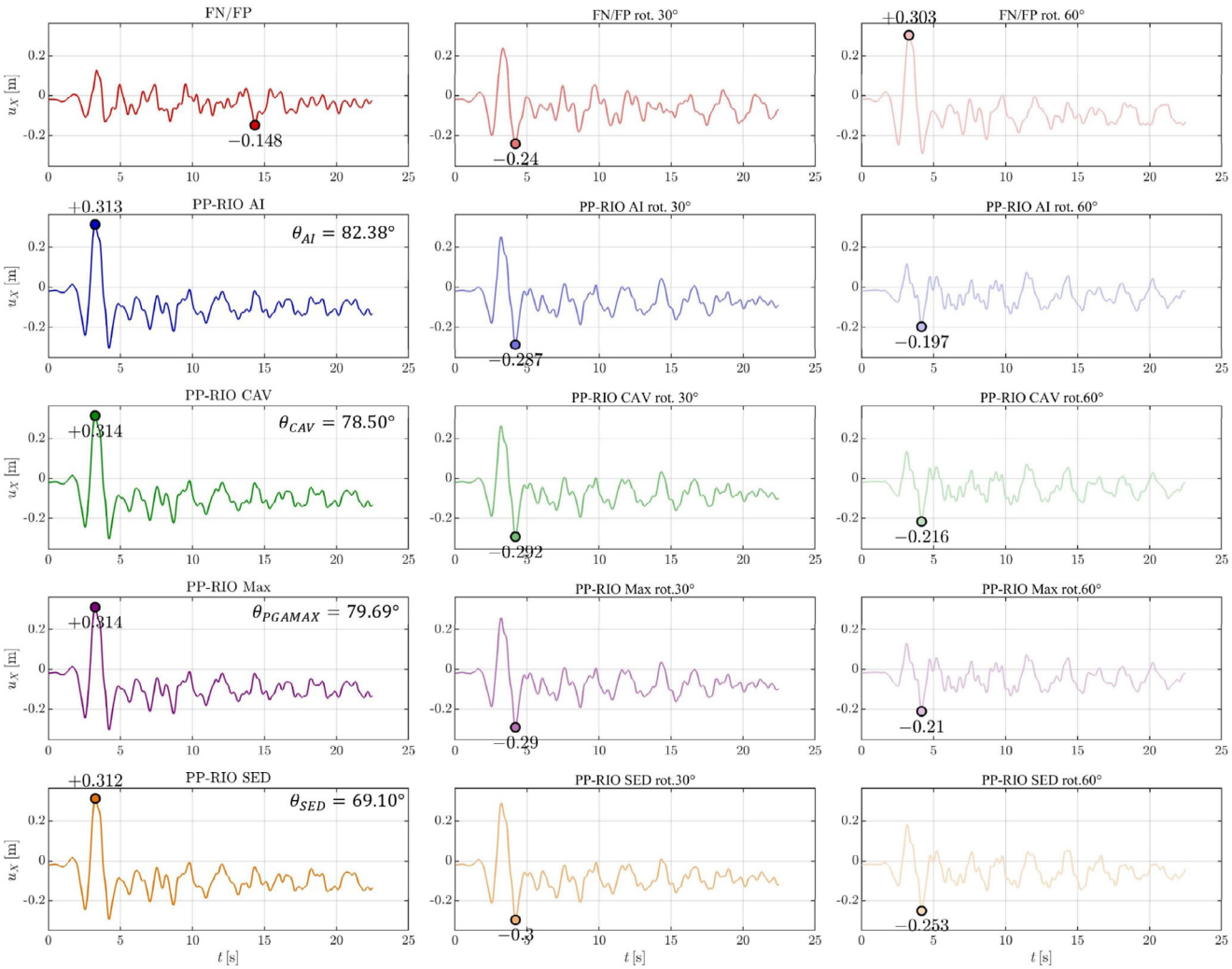

FIGURE 9 | Response displacement time history in the X-direction for Record ID 034. The peak structural demand identified by the PP-RIO metrics (*PP-RIO* CAV/AI) has been observed to significantly exceed the values obtained from the standard fault-aligned protocol (*FN/FP*).

of the structural demand, ensuring that the critical energy flux and displacement demands are accounted for in the NLTHA design process. Consequently, as evidenced in the displacement performance metric and confirmed by the storey drift profile, rotating an arbitrary angle from the PP-RIO-derived IM directions (e.g., *PP-RIO SED rot.30* or *PP-RIO Max rot.60*) yields a non-conservative response, further confirming the effectiveness of the PP-RIO methodology.

8 | PP-RIO Performance in NLTHA

Following the detailed examination of the illustrative case study in Section 7, the discussion is expanded to a representative sample of the dataset comprising PL, NF, and FF ground motion records. This global analysis aims to statistically validate the efficacy of the proposed PP-RIO methodology against standard practice (FN/FP) and arbitrary geometric rotations. The assessment integrates the spectral characteristics of the excitation with the resulting EDP to isolate the effects of ground motion regime and structural resonance.

8.1 | Dominant Frequency Characteristics and Pulse–Structure Compatibility

Figure 11 presents the dominant frequency (f_{dom}) of the Fault-Normal (FN) acceleration component for the *PL*, *NF*, and *FF* datasets, together with the fundamental frequency of the structure in the X direction (f_{struct} = 0.5506 Hz, dashed line). The FN component is shown because, in the baseline fault-aligned configuration adopted in the analyses, it is assigned to the structural X direction. The dominant frequency was computed as the frequency corresponding to the maximum ordinate of the Fourier amplitude spectrum of the selected acceleration component.

A substantial variability of dominant frequency is observed within the PL regime (Records 1–15). Several records exhibit dominant frequencies well above the fundamental frequency of the structure, whereas others, such as Record 3 and Record 14, present values close to f_{struct}. This proximity should not be interpreted as classical dynamic resonance, since pulse-like records are generally characterized by one or a few dominant pulses. Pulse-period compatibility provides a more appropriate

10969845, 0, Downloaded from https://onlinelibrary.wiley.com/doi/10.1002/eqe.70286 by Marco Domaneschi - Politecnico Di Torino Sist. Bibl Del Polit Di Torino , Wiley Online Library on [26/08/2026]. See the Terms and Conditions (https://onlinelibrary.wiley.com/terms-and-conditions) on Wiley Online Library for rules of use; OA articles are governed by the applicable Creative Commons License

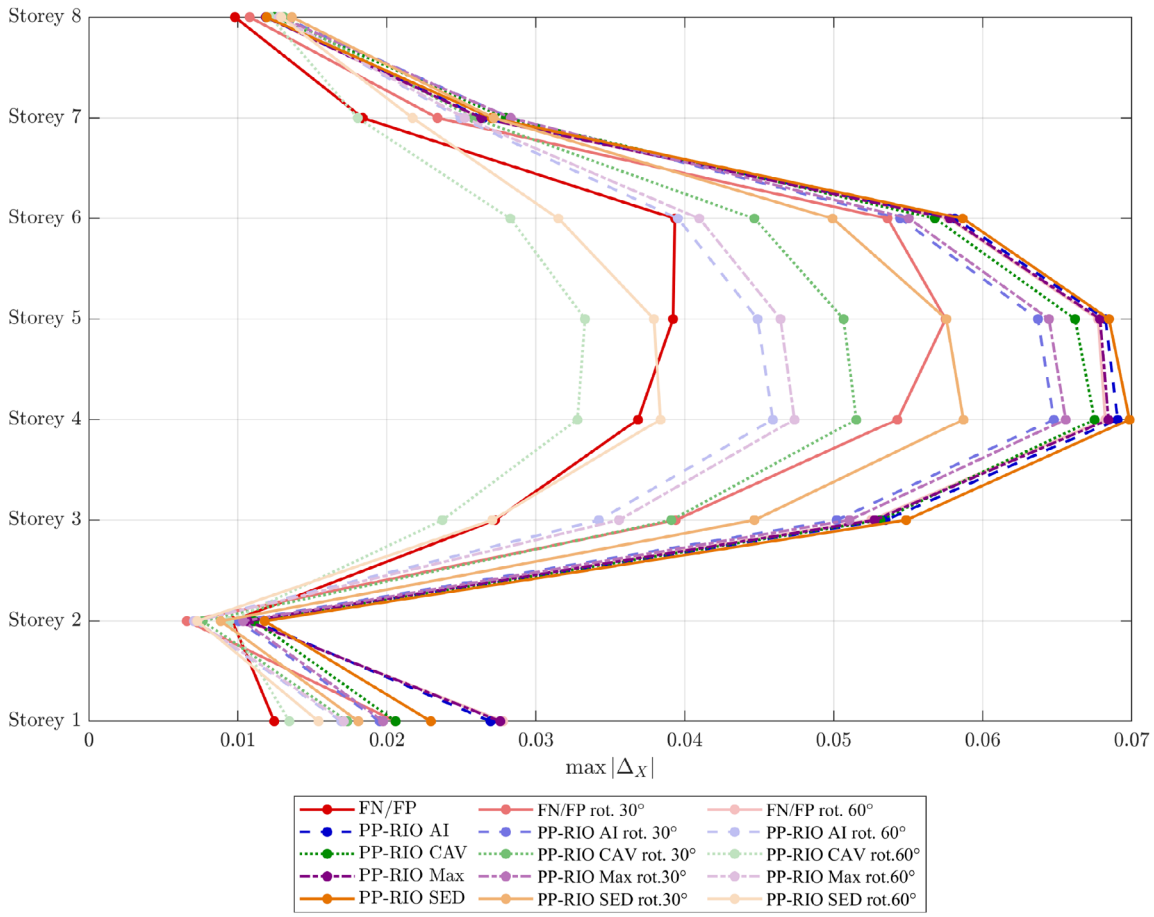

FIGURE 10 | Vertical profiles of maximum storey drift ratios (SDR) for Record ID 034. The standard orientation is observed to underestimate the deformation demand (≈ 3.9%) compared to the Intensity-based PP-RIO orientations which reveal critical drifts reaching ≈ 7.0%.

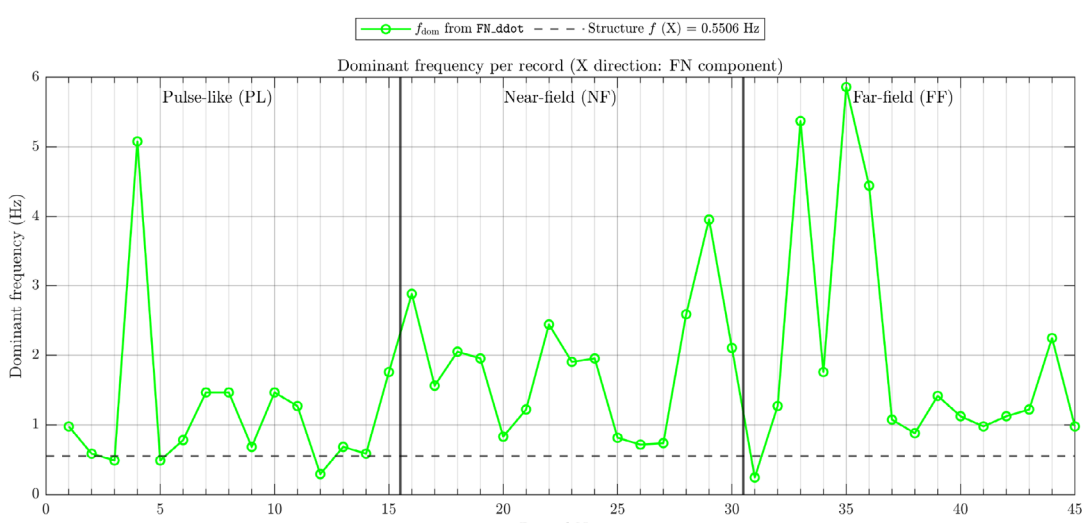

FIGURE 11 | Distribution of dominant frequencies (f_{dom}) for the FN component across the analyzed datasets. The fundamental structural frequency (f_{struct} = 0.5506 Hz) is denoted by the dashed line, highlighting potential pulse-period compatibility conditions particularly within specific events in the PL regime.

10969845, 0, Downloaded from https://onlinelibrary.wiley.com/doi/10.1002/eqe.70286 by Marco Domaneschi - Politecnico Di Torino Sist. Bibl Del Polit Di Torino , Wiley Online Library on [26/08/2026]. See the Terms and Conditions (https://onlinelibrary.wiley.com/terms-and-conditions) on Wiley Online Library for rules of use; OA articles are governed by the applicable Creative Commons License

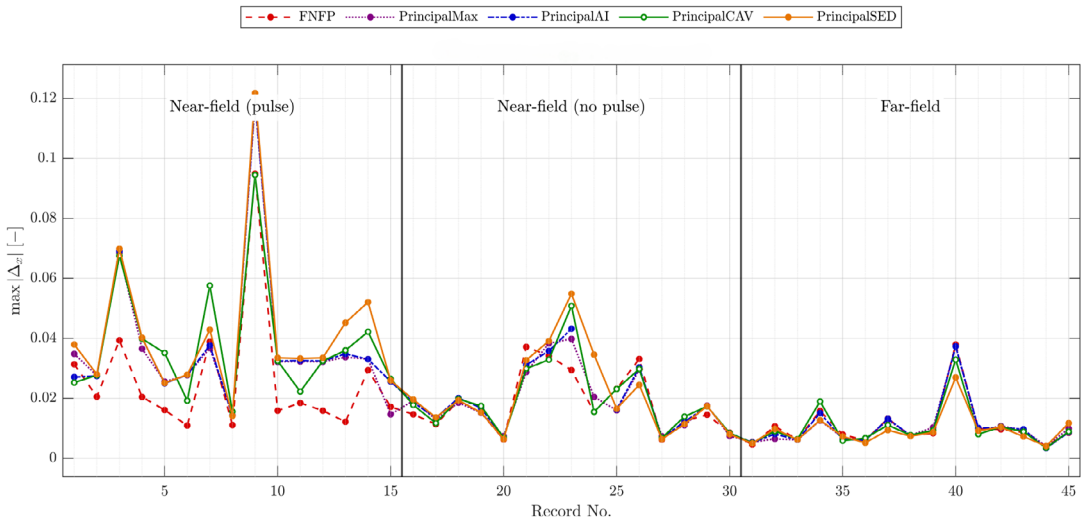

FIGURE 12 | Global comparison of maximum X-direction storey drift (max $|\Delta_x|$) across all records. Note the critical divergence in the Pulse-Like regime (e.g., Record 9), where standard recording orientations significantly underestimate the potential demand identified by principal metrics.

interpretation. When $T_p > T_n$, yielding-induced period elongation may amplify displacement and energy demands, with severe inelastic response often reported for $T_p/T_n \approx 1.5$–2.5 [27–30].

Therefore, if any, and for few of the selected PL events, the increased response observed for selected pulse-like records is interpreted here as the result of pulse-period compatibility with the nonlinear structural period range, but also combined with the strong polarization of the input motion. Conversely, the NF and FF records generally exhibit more dispersed frequency content and, in several cases, dominant frequencies farther from the fundamental structural frequency. Nevertheless, the subsequent EDP trends indicate that the observed demand variations cannot be explained by frequency content alone. Even when the dominant frequency is not close to f_{struct}, the orientation of the dominant intensity or energy flux relative to the structural axes may significantly modify the nonlinear response. Thus, Figure 11 provides useful background information on the spectral characteristics of the selected records, while the role of directionality is evaluated directly through the rotated bidirectional NLTHA results discussed in the following sections.

8.2 | Comparative Assessment of EDP Metrics

The distribution of the Maximum SDR among the different records is illustrated in Figures 12 and 13. These figures facilitate a multi-dimensional comparison between the fault-aligned orientation FN/FP, arbitrary fixed-angle rotations, and the Intensity-based PP-RIO orientations.

8.2.1 | Storey Drift Response

In the FF domain (Records 31-45, Figure 12), the response envelopes for all methodologies tend to converge, corroborating the hypothesis of wavefield isotropization at larger source-to-site distances. In addition, the penalty associated with an arbitrary sensor orientation is minimal. However, a critical difference characterizes the PL domain (Records 1–15). Here, the FN/FP protocol (red dashed line) frequently underestimates the demand compared to the intensity-aligned orientations (solid lines). This is most notably observed in Record 9, where the structure undergoes extreme nonlinear demand. While the fault-aligned component suggests a drift of approximately 8%, the PP-RIO metrics reveal a critical excursion exceeding 12% (see Figure 13). In such cases, the PP-RIO metrics, particularly those based on SED and CAV, consistently track the upper bound of the structural response, ensuring that the directional energy associated with the maximum damage potential is captured.

8.2.2 | Arbitrary Geometric Rotations

The limitation of arbitrary geometric approaches is also presented in Figure 13. The comparison between fixed rotations (30°, 60°) and the Specific Energy Density (*PP-RIO SED*) orientation reveals significant volatility. While fixed rotations (faint orange lines) occasionally exceed the FN/FP demand, they lack a physical basis and often fail to capture the true maximum, falling below the envelope defined by the *PP-RIO SED* orientation (solid orange line). This is evident in Record 23 (NF), where the SED-based orientation successfully identifies a peak demand ($\approx 5.5\%$) that exceeds both the fault-aligned and fixed-rotation protocols, the previous reflection is even more emphasized for the PL records. Consequently, relying on fixed rotations is statistically equivalent to an arbitrary sampling of the hazard, whereas the PP-RIO protocols provide a deterministic identification of the critical loading angle.

8.3 | Statistical Robustness of Directionality Indices

To rigorously quantify the reliability of the proposed methodology, the directionality efficiency index, η_{Axis}, is evaluated. It measures the fraction of the peak resultant response that can be captured by a single (most-demanding) horizontal axis, i.e., the

10969845, 0, Downloaded from https://onlinelibrary.wiley.com/doi/10.1002/eqe.70286 by Marco Domaneschi - Politecnico Di Torino Sist. Bibl Del Polit Di Torino , Wiley Online Library on [26/08/2026]. See the Terms and Conditions (https://onlinelibrary.wiley.com/terms-and-conditions) on Wiley Online Library for rules of use; OA articles are governed by the applicable Creative Commons License

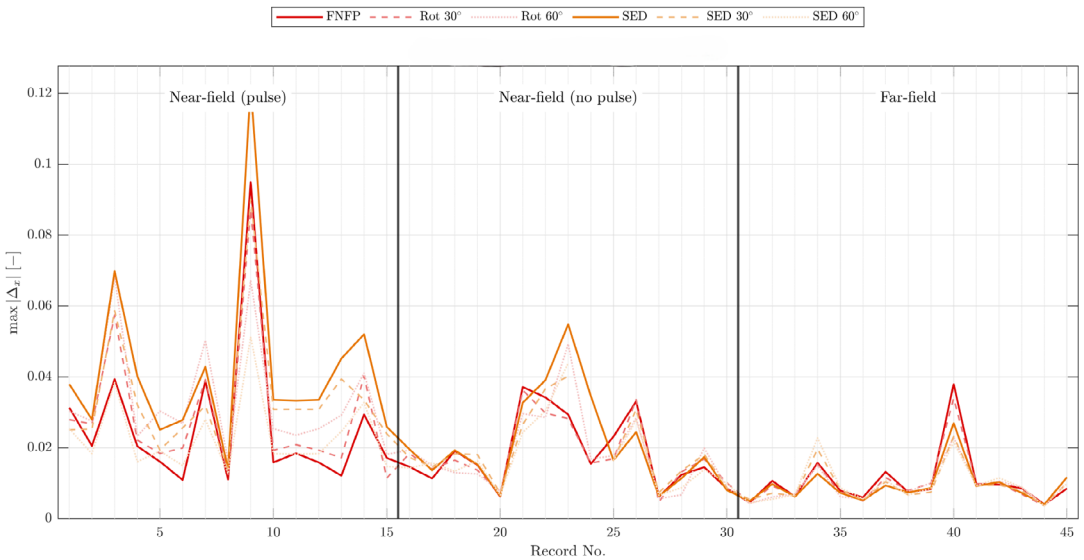

FIGURE 13 | Comparison of Maximum Storey Drift in X between standard approaches (FNFP, Rot 30°/60°) and the Intensity-based PP-RIO protocol (*PP-RIO SED*). The SED methodology consistently envelopes the demand, whereas fixed rotations exhibit volatile performance.

degree of alignment of the peak response vector with the nearest reference axis. It is defined at the instant of maximum resultant demand as shown in Equation (7)

$$\eta_{\text{Axis}} = \left.\frac{\max\left(|u_x|,\ |u_y|\right)}{\sqrt{u_x^2 + u_y^2}}\right|_{t=t_{\text{peak}}}, \qquad t_{\text{peak}} = \arg\max_t \sqrt{u_x^2(t) + u_y^2(t)}, \tag{7}$$

where $u_x(t)$ and $u_y(t)$ denote the instantaneous horizontal displacement responses of the top-floor control node, along the two orthogonal structural axes X and Y, respectively. Accordingly, t_{peak} corresponds to the time instant at which the resultant roof displacement reaches its maximum value. With $1/\sqrt{2} \leq \eta_{\text{Axis}} \leq 1$, values approaching unity indicate that the peak resultant response is predominantly aligned with one structural axis, whereas values close to $1/\sqrt{2}$ indicate comparable contributions from both horizontal components.

Figure 14 presents the quantile bands of η_{Axis} for the top-floor displacement response. The standard FN/FP orientation exhibits a wide interquartile range with a lower whisker extending below $\eta_{\text{Axis}} = 0.85$, statistically confirming that random sensor orientation introduces a significant probability of unconservative error. Crucially, the arbitrary rotations ($Rotated30°$, $Rotated60°$) display even greater dispersion and lower median values than the fault-aligned baseline in some instances, reinforcing their unsuitability for reliability-based design. In distinct contrast, the PP-RIO protocols relying on robust IM, specifically Cumulative Absolute Velocity (*PP-RIO CAV*) and Specific Energy Density (*PP-RIO SED*), demonstrate superior performance. The *PP-RIO SED* metric (Orange box), in particular, exhibits the tightest distribution with a median approaching unity and negligible variance. This suggests that for PL ground motions, cumulative energy metrics are more robust predictors of the critical structural response axis than instantaneous peak measures like PGA (*PP-RIO Max*). By integrating the energy content over the duration of the record, SED effectively aligns the structural axes with the direction of maximum damage potential, minimizing the epistemic uncertainty associated with load orientation.

8.4 | EDP Directional Response Sensitivity

Further EDP-based comparisons discussed in the previous sections, the directional distribution of the peak structural response is examined for the Pulse-Like subset. Figure 15 reports polar histograms of the response angle associated with the peak resultant top-floor displacement. In contrast to the balanced subset of 15 records per regime used for the direct FF–NF–PL comparisons, this analysis was performed using the complete PL subset available in the database ($N = 69$). The purpose is not to compare different seismological regimes, but to assess whether the directional clustering observed for PL motions persists when a larger set of pulse-like records is considered. The response angle is defined at the instant of maximum resultant roof displacement, i.e., at the time instant where $\sqrt{u_x^2(t) + u_y^2(t)}$ reaches its maximum value. Therefore, the polar histograms describe the direction in which the peak displacement vector develops under each orientation protocol. Since polar histograms are sensitive to sample size and binning, the results are interpreted as evidence of directional tendencies within the PL subset rather than as a deterministic classification of response direction.

The first column illustrates the baseline directional content of the response. Under the geometric *FN/FP* orientation, the polar histogram exhibits a scattered, multi-lobed pattern distributed across several angular sectors. This indicates that, within the PL regime, the peak resultant displacement is attained at orientations that are not stably related to the loading axes; consequently, the apparent critical direction depends strongly on the arbitrary choice of reference system. Conversely, for the PP-RIO cases (IM-driven rotations), the distributions become progressively more concentrated, indicating that the response direction is no

10969845, 0, Downloaded from https://onlinelibrary.wiley.com/doi/10.1002/eqe.70286 by Marco Domaneschi - Politecnico Di Torino Sist. Bibl Del Polit Di Torino , Wiley Online Library on [26/08/2026]. See the Terms and Conditions (https://onlinelibrary.wiley.com/terms-and-conditions) on Wiley Online Library for rules of use; OA articles are governed by the applicable Creative Commons License

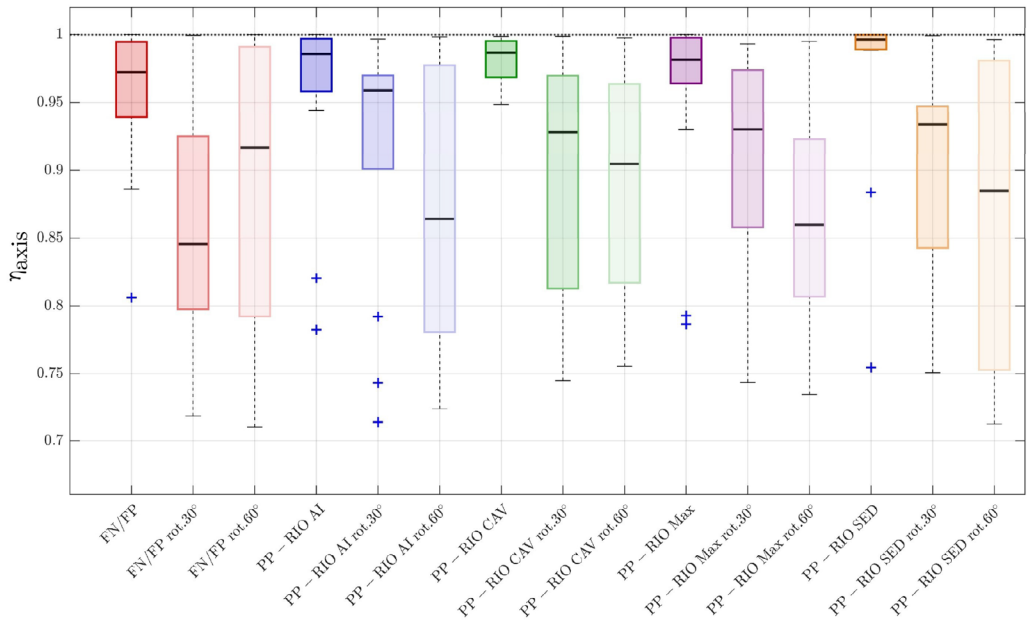

FIGURE 14 | Quantile bands of the directionality efficiency index η for top-floor displacement. The compact distributions for integral IM, particularly the SED and CAV, based protocols indicate a statistically superior capability to capture the maximum structural demand and lower dispersion compared to geometric fixed-rotations (30°/60°) or *FN/FP* PGA-based (PP-RIO Max) methods.

longer coordinate-dependent but converges toward a preferred orientation induced by the Intensity-based alignment.

The influence of arbitrary rotations becomes evident when comparing the second and third columns (rotated by 30° and 60°). For the *FN/FP* geometric rotations (top row), the dominant lobes shift substantially with rotation: the angular distribution changes shape and the peak sectors migrate, demonstrating strong sensitivity of the inferred response direction to the adopted coordinate frame. In contrast, the PP-RIO rows display a markedly reduced dependence on the imposed rotation: the principal response sector remains comparatively stable, and the redistribution of counts is limited, although minor shifts and partial loss of alignment are still observed. This behavior indicates that the PP-RIO framework promotes an almost invariant estimate of the structural principal response direction, consistent with the objective of identifying a physically meaningful wavefront-driven axis.

A row-by-row inspection further reveals how the choice of IM within PP-RIO affects the stability of the response direction. The *PP-RIO AI* row already exhibits a clear reduction in entropy relative to the *FN/FP*, but residual secondary lobes remain, suggesting partial convergence. The *PP-RIO CAV* and PP-RIO Max rows show a stronger clustering, with a dominant lobe emerging and secondary contributions becoming less pronounced, indicating an increased consistency of the response angle associated with the peak displacement. The most pronounced directional convergence is observed for *PP-RIO SED*, where the distribution collapses into a narrow angular sector. This strong clustering implies that, when the input is aligned according to an Intensity-based IM, the structural response becomes directionally stable and predominantly governed by a well-defined axis of maximum energy delivery, yielding the lowest directional variability among the considered PP-RIO definitions.

9 | Conclusions and Future Developments

This study proposed the PP-RIO methodology as a deterministic, intensity-measure-based orientation criterion for bidirectional ground motions in NLTHA. The method is intended as a complementary orientation check to fault-aligned, sensor-based, or fixed-rotation protocols. It is not proposed as a universal replacement for current record-orientation procedures, but as a reproducible way to investigate whether aligning the maximum-intensity direction of a selected ground motion with a principal structural axis can reveal larger nonlinear deformation demands otherwise neglected or overlooked.

By transitioning from arbitrary geometric rotations to Intensity-based intensity alignments, the influence of seismic incidence angle on the nonlinear response of a broadly adopted reinforced concrete low- to mid-rise structure has been systematically quantified. This formulation has thereby isolated the impact of directionality across distinct seismological regimes, yielding the following conclusions:

- For the investigated eight-storey reinforced concrete frame, the results indicate that PP-RIO orientations may lead to larger deformation demands than the fault-aligned FN/FP orientation, especially for pulse-like near-fault records. In the representative Pulse-Like case ID_034 examined in detail, the maximum storey drift increased from approximately 3.9% under the FN/FP orientation to approximately 7.0% under the PP-RIO-based orientation, while the maximum roof displacement increased from approximately 0.148 m to approximately 0.314 m, with consistent metrics for the other cases. These values illustrate the potential magnitude of the orientation effect for a directionally concentrated record, but they should not be interpreted as generalized amplification

10969845, 0, Downloaded from https://onlinelibrary.wiley.com/doi/10.1002/eqe.70286 by Marco Domaneschi - Politecnico Di Torino Sist. Bibl Del Polit Di Torino , Wiley Online Library on [26/08/2026]. See the Terms and Conditions (https://onlinelibrary.wiley.com/terms-and-conditions) on Wiley Online Library for rules of use; OA articles are governed by the applicable Creative Commons License

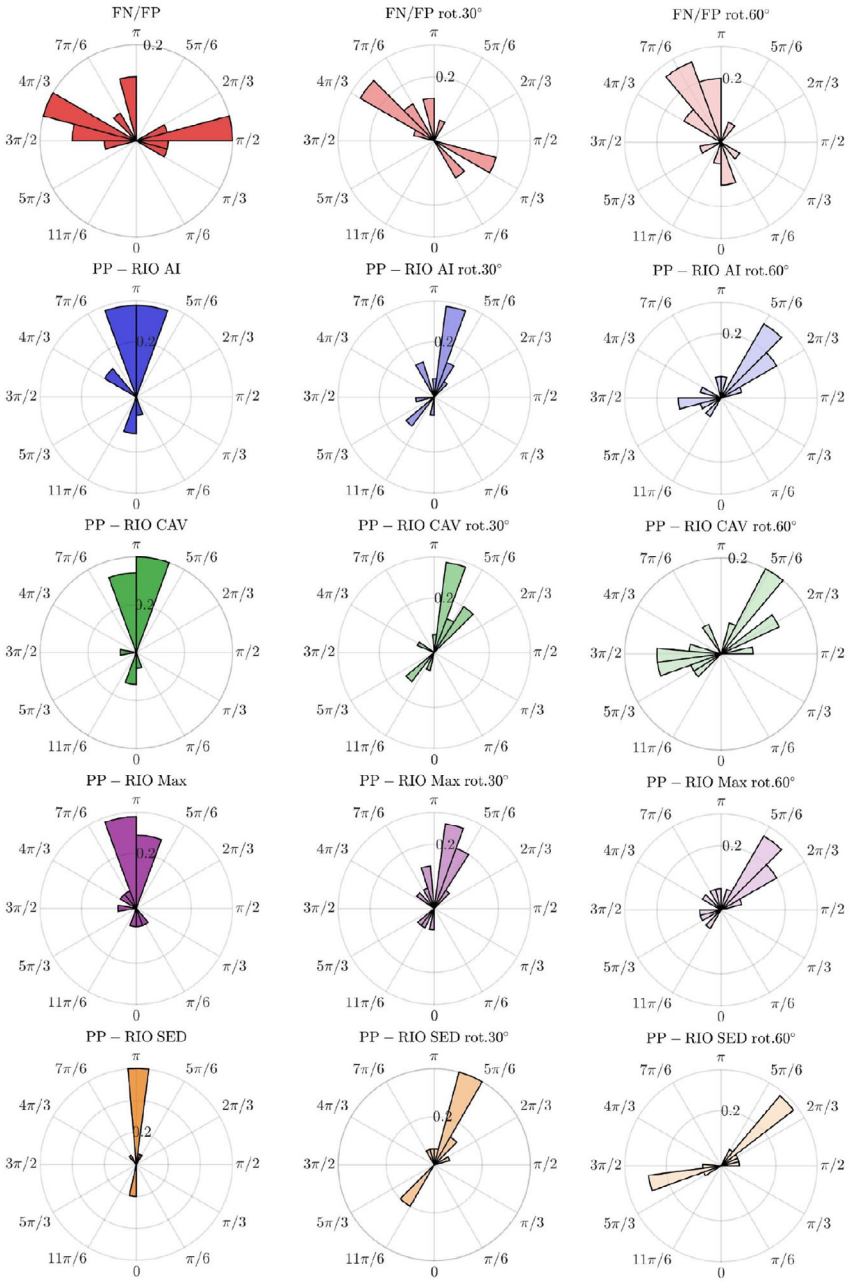

FIGURE 15 | Polar histograms of the response angle associated with the peak resultant top-floor displacement for the complete Pulse-Like dataset ($N = 69$). The response angle is evaluated at the time instant at which the resultant roof displacement reaches its maximum value. Rows correspond to the fault-aligned FN/FP protocol and to the PP-RIO orientations derived from different scalar IMs, while columns show the reference orientation and additional rotations of 30° and 60°. The broader, multi-lobed distributions observed for the geometric FN/FP-based protocols indicate greater sensitivity of the peak response direction to the adopted reference frame. In contrast, the PP-RIO protocols show increased directional clustering, particularly for the SED-based orientation, suggesting a more stable alignment between the intensity-based input direction and the resulting structural response.

factors, as further studies should be performed considering different structural configurations.

- The application of the Peak-Polar Rotation-Intensity methodology effectively mitigates the epistemic uncertainty associated with arbitrary sensor orientation. The standard Fault-Normal/Fault-Parallel protocol, while widely adopted in engineering practice, has been statistically demonstrated to yield unconservative estimates of structural demand. This divergence is regime-dependent: while Far-Field records exhibit a tendency toward isotropic response, the Pulse-Like Near-Field regime reveals critical vulnerabilities. In specific cases (e.g., Record 09 in Figure 13), the standard orientation underestimated the maximum storey drift ratio compared to the critical direction. Consequently, reliance on fault-aligned components in proximity to seismic sources introduces a latent risk of unpredicted failure mechanisms.
- The comparative analysis of fixed geometric rotations with respect to the Intensity-based reference system (e.g., *PP-RIO*

10969845, 0, Downloaded from https://onlinelibrary.wiley.com/doi/10.1002/eqe.70286 by Marco Domaneschi - Politecnico Di Torino Sist. Bibl Del Polit Di Torino , Wiley Online Library on [26/08/2026]. See the Terms and Conditions (https://onlinelibrary.wiley.com/terms-and-conditions) on Wiley Online Library for rules of use; OA articles are governed by the applicable Creative Commons License

SED rotated by 30° and 60°) reveals that such protocols fail to provide a consistent reliability margin. As evidenced by the dispersion in the directionality efficiency index (η_{Axis}), these arbitrary rotations function as a non-physical sampling process rather than a targeted maximization strategy. They typically exhibit high variability and, in numerous instances, fail to capture the global drift envelope correctly identified by Intensity-based methods. Therefore, simply adding rotated load cases without seismological justification increases computational cost without ensuring reliable identification of the critical demand direction.

- Among the scalar IMs examined, the metrics based on cumulative energy, specifically Specific Energy Density (*PP-RIO SED*) and Cumulative Absolute Velocity (*PP-RIO CAV*), exhibit remarkable stability and predictive capability compared to polar peak-based metrics such as PGA (*PP-RIO Max*). The statistical analysis of the efficiency index (η) demonstrates that SED-based orientations consistently yield median values approaching unity ($\eta \approx 1.0$) with negligible interquartile variance. This indicates that, by accounting for cumulative damage potential and shaking duration, intensity-based metrics effectively filter out high-frequency, non-damaging acceleration spikes that often skew *PGA*-based maximizations.
- Overall, the directionality sensitivity of the structural response exhibits two coupled trends: (i) *FN/FP* protocols yield response-angle distributions that vary markedly with the arbitrary choice (and rotation) of the reference system; and (ii) Intensity-based Peak-Polar Rotation-Intensity alignments substantially mitigate this dependence, steering the response toward a stable principal direction. The resulting angular concentration of the studied dataset should be interpreted as a reduction in the *directional uncertainty* of the peak *EDP*, supporting the conclusion that the Peak-Polar Rotation-Intensity methodology captures the physical directionality of the seismic input and its coherent manifestation in structural response.

Although the Peak-Polar Rotation-Intensity methodology has been validated for a regular reinforced concrete frame, its generalization to irregular, torsionally sensitive, and typologically diverse structural systems requires further investigation to assess the robustness of integral-based IMs across varying dynamic characteristics and material behaviors. Future research will extend the proposed methodology toward broader structural classes and larger record datasets, incorporating direction-dependent ductility and fiber-level strain response and pointing to contribute on the codification of Intensity-based rotation protocols within nonlinear time-history and performance-based design guidelines.

Author Contributions

Santiago Londono-Lopez: Data curation, formal analysis, investigation, methodology, software, validation, visualization, writing – original draft, writing – review and editing. **Raffaele Cucuzza**: Methodology, supervision, validation, visualization, writing – original draft, writing – review and editing. **Fabrizio Mollaioli**: Conceptualization, data curation, methodology, resources, writing – review and editing. **Giuseppe Carlo Marano**: Conceptualization, methodology, resources, writing – review and editing. **Marco Domaneschi**: Conceptualization, funding acquisition, methodology, project administration, supervision, validation, visualization, writing – original draft, writing – review and editing.

Acknowledgments

The research leading to these results has received funding from (i) the European Union under the Project PNRR - MUR DM 118 - CUP E14D23001710006118/2023, and (ii) "The support given by PRIN 2022" BIO-RESTORE– BIO-based Resilient Energy and Seismic retrofiT Of the REsidential building stock", Prot. 202234HM8J, CUP E53C24002680006, Bando Prin 2022 - Decreto Direttoriale n. 104 del 02-02-2022 part of the project "National Recovery and Resilience Plan-Next Generation EU" (PNRR-NGEU) which has received funding from the Italian Ministry of University and Research (MUR) – DM 629/2024 is gratefully acknowledged.

Open access publishing facilitated by Politecnico di Torino, as part of the Wiley - CRUI-CARE agreement.

Conflicts of Interest

The authors declare no conflicts of interest.

Data Availability Statement

The data that support the findings of this study are available from the corresponding author upon reasonable request.

References

1. F. Porcelli and R. Trezzi, "The Impact of Earthquakes on Economic Activity: Evidence From Italy," *Empirical Economics* 56 (2019): 1167–1206.

2. M. Domaneschi, R. Cucuzza, L. Martinelli, et al., "A Probabilistic Framework for the Resilience Assessment of Transport Infrastructure Systems via Structural Health Monitoring and Control Based on a Cost Function Approach," *Structure and Infrastructure Engineering* 22, no. 1 (2024): 107–119, https://doi.org/10.1080/15732479.2024.2318231.

3. F. Perotti, M. Domaneschi, and S. D. Grandis, "The Numerical Computation of Seismic Fragility of Base-Isolated Nuclear Power Plants Buildings," *Nuclear Engineering and Design* 262 (2013): 189–200.

4. R. Westaway, "Seismic Moment Summation for Historical Earthquakes in Italy: Tectonic Implications," *Journal of Geophysical Research* 97 (1992): 15437–15464.

5. K. Kostinakis, A. Athanatopoulou, and I. Avramidis, "Orientation Effects of Horizontal Seismic Components on Longitudinal Reinforcement in R/C Frame Elements," *Natural Hazards and Earth System Sciences* 12, no. 1 (2012): 1–10.

6. M. A. Hussain, S. C. Dutta, S. Das, et al., "Influence of Post-Elastic Range Bidirectional Interaction for Various Angles of Incidence of Ground Motions on One-Story Asymmetric Structures," *Journal of Earthquake Engineering* 27 (2023): 4527–4548.

7. O. A. López and R. Torres, "The Critical Angle of Seismic Incidence and the Maximum Structural Response," *Earthquake Engineering & Structural Dynamics* 26, no. 9 (1997): 881–894.

8. K. Kostinakis, A. Athanatopoulou, and K. Morfidis, "Correlation Between Ground Motion Intensity Measures and Seismic Damage of 3d R/C Buildings," *Engineering Structures* 82 (2015): 151–167.

9. D. Skoulidou and X. Romão, "The Significance of Considering Multiple Angles of Seismic Incidence for Estimating Engineering Demand Parameters," *Bulletin of Earthquake Engineering* 18, no. 1 (2020): 139–163.

10. P. E. Sebastiani, L. Liberatore, A. Lucchini, F. Mollaioli, et al., "Simple Models to Predict the Most Critical Incidence Angle for Buildings Under Bi-Directional Near-Fault Excitations," in *Second European Conference on Earthquake Engineering and Seismology* (European Seismological Commission, 2014).

10969845, 0, Downloaded from https://onlinelibrary.wiley.com/doi/10.1002/eqe.70286 by Marco Domaneschi - Politecnico Di Torino Sist. Bibl Del Polit Di Torino , Wiley Online Library on [26/08/2026]. See the Terms and Conditions (https://onlinelibrary.wiley.com/terms-and-conditions) on Wiley Online Library for rules of use; OA articles are governed by the applicable Creative Commons License

11. D. M. Boore, J. Watson-Lamprey, and N. A. Abrahamson, "Orientation-Independent Measures of Ground Motion," *Bulletin of the seismological Society of America* 96, no. 4A (2006): 1502–1511.

12. D. M. Boore, "Orientation-Independent, Nongeometric-Mean Measures of Seismic Intensity From Two Horizontal Components of Motion," *Bulletin of the Seismological Society of America* 100, no. 4 (2010): 1830–1835.

13. T. D. Ancheta, R. B. Darragh, J. P. Stewart, et al., "NGA-West2 database," *Earthquake Spectra* 30, no. 3 (2014): 989–1005.

14. National Research Institute for Earth Science and Disaster Resilience, *NIED Strong-motion Network (K-NET, KiK-net)* (2019).

15. L. Luzi, R. Puglia, E. Russo, et al., "The Engineering Strong-Motion Database: A New International Resource for Engineering Seismology," *Seismological Research Letters* 87, no. 6 (2016): 1467–1478.

16. F. Pacor, R. Paolucci, R. Puglia, et al., "The Italian Accelerometric Archive (ITACA): Processing and Database of Strong-Motion Signals," *Bulletin of Earthquake Engineering* 9, no. 6 (2011): 1891–1922.

17. S. Akkar, Z. Çağnan, G. Yenier, Ö. Erdoğan, M. A. Sandıkkaya, and P. Gülkan, "The Turkish Strong-Motion Database in Updated Form and a Compiled Levant Region Strong-Motion Data Set," *Bulletin of Earthquake Engineering* 8, no. 3 (2010): 527–558.

18. A. B. Rigato and R. A. Medina, "Influence of Angle of Incidence on Seismic Demands for Inelastic Single-Storey Structures Subjected to Bi-Directional Ground Motions," *Engineering Structures* 29, no. 10 (2007): 2593–2601.

19. E. L. Wilson and M. R. Button, "Three-Dimensional Dynamic Analysis for Multi-Component Earthquake Spectra," *Earthquake Engineering & Structural Dynamics* 10, no. 3 (1982): 471–476.

20. C. Menun and A. Der Kiureghian, "A Replacement for the 30%, 40%, and SRSS Rules for Multicomponent Seismic Analysis," *Earthquake Spectra* 14, no. 1 (1998): 153–163.

21. J. C. Reyes and E. Kalkan, *Should Ground-Motion Records be Rotated to Fault-Normal/Parallel or Maximum direction for Response History Analysis of Buildings?* US Geological Survey, Technical Report (USGS, 2012).

22. K. Kostinakis, A. Athanatopoulou, and I. Avramidis, "Evaluation of Inelastic Response of 3D Single-Story R/C Frames Under Bi-Directional Excitation Using Different Orientation Schemes," *Bulletin of Earthquake Engineering* 11, no. 2 (2013): 637–661.

23. I.-K. M. Fontara, K. G. Kostinakis, G. E. Manoukas, and A. M. Athanatopoulou, "Parameters Affecting the seismic response of buildings under bi-directional excitation," *Structural Engineering and Mechanics* 53, no. 5 (2015): 957–979.

24. C. Cantagallo, G. Camata, and E. Spacone, "Influence of Ground Motion Selection Methods on Seismic Directionality Effects," *Earthquakes and Structures* 8, no. 1 (2015): 185–204.

25. A. Rivera-Figueroa and L. A. Montejo, "Spectral Matching RotD100 Target Spectra: Effect on Records Characteristics and Seismic Response," *Earthquake Spectra* 38, no. 2 (2022): 1570–1586.

26. A. Rivera-Figueroa, L. A. Montejo, and D. N. Grant, "Spectral Matching RotD100: Effects on Bidirectional Lateral Demand of Reinforced Concrete Frame Buildings," *Earthquake Spectra* 39, no. 4 (2023): 2664–2684.

27. B. Alavi and H. Krawinkler, "Behavior of Moment-Resisting Frame Structures Subjected to Near-Fault Ground Motions," *Earthquake Engineering & Structural Dynamics* 33, no. 6 (2004): 687–706.

28. C. Champion and A. Liel, "The Effect of Near-Fault Directivity on Building Seismic Collapse Risk," *Earthquake Engineering & Structural Dynamics* 41, no. 10 (2012): 1391–1409.

29. X. Roman-Velez and L. A. Montejo, "Generation of Seed-Based Spectrum-Compatible Pulse-Like Time-Series," *Bulletin of Earthquake Engineering* 18, no. 4 (2020): 1161–1186.

30. L. A. Montejo, "Spectrally Matching Pulse-Like Records to a Target RotD100 Spectrum," *Earthquake Engineering & Structural Dynamics* 52, no. 9 (2023): 2796–2811.

31. H. P. Hong and K. Goda, "Characteristics of Horizontal Ground Motion Measures Along Principal Directions," *Earthquake Engineering and Engineering Vibration* 9 (2010): 9–22.

32. J. W. Baker, "Quantitative Classification of Near-Fault Ground Motions Using Wavelet Analysis," *Bulletin of the seismological society of America* 97, no. 5 (2007): 1486–1501.

33. H. Sato, M. C. Fehler, and T. Maeda, *Seismic Wave Propagation and Scattering in the Heterogeneous Earth* (Springer, 2012), 496.

34. S. Crampin, "A Review of the Effects of Anisotropic Layering on the Propagation of Seismic Waves," *Geophysical Journal International* 49, no. 1 (1977): 9–27.

35. S. K. Shahi and J. W. Baker, "NGA-West2 Models for Ground Motion Directionality," *Earthquake Spectra* 30, no. 3 (2014): 1285–1300.

36. B. Kennett, *Seismic Wave Propagation in Stratified Media* (ANU Press, 2009).

37. P. E. Sebastiani, L. Liberatore, A. Lucchini, and F. Mollaioli, "A New Method to Predict the Critical Incidence Angle for Buildings Under Near-Fault Motions," *Structural Engineering and Mechanics* 68, no. 5 (2018): 575–589.

38. OpenSees Development Team- PEER, *OpenSees: Open System for Earthquake Engineering Simulation*. Accessed November 11, 2025.

39. R. Zhang, Z. Sun, and C. Qu, "P-Delta Effects on Nonlinear Dynamic Response of Steel Moment-Resisting Frame Structures Subjected to Near-Fault Pulse-Like Ground Motions," in *Structures*, vol. 41 (Elsevier, 2022), 1122–1140.

40. B. Mohebi, F. Kazemi, and M. Yakhchalian, "Investigating the P-Delta Effects on the Seismic Collapse Capacity of Adjacent Structures," in *16th European Conference on Earthquake Engineering (16ECEE)* (2018), 18–21.

41. A. Arias, "A Measure of Earthquake Intensity," in *Seismic Design for Nuclear Power Plants*, R. J. Hansen, Ed. (MIT Press, 1970), 438–483.

42. Electric Power Research Institute, *A Criterion for Determining Exceedance of the Operating Basis Earthquake*, Palo Alto, CA, Technical Report NP-5930 (EPRI, 1988).

43. S. K. Sarma, "Energy Flux of Strong Earthquakes," *Tectonophysics* 11, no. 3 (1971): 159–172.

10969845, 0, Downloaded from https://onlinelibrary.wiley.com/doi/10.1002/eqe.70286 by Marco Domaneschi - Politecnico Di Torino Sist. Bibl Del Polit Di Torino , Wiley Online Library on [26/08/2026]. See the Terms and Conditions (https://onlinelibrary.wiley.com/terms-and-conditions) on Wiley Online Library for rules of use; OA articles are governed by the applicable Creative Commons License